Guiding epitaxial crystallization of amorphous solids at the nanoscale: interfaces, stress, and precrystalline order

T. Janicki,[1] Z. Wan,[1] R. Liu,[2] P. G. Evans,[2, a)] and J. R. Schmidt[1, b)]

[1)]*Department of Chemistry, University of Wisconsin-Madison, Madison, WI 53706, USA*

[2)]*Department of Materials Science and Engineering, University of Wisconsin-Madison, Madison, WI 53706, USA*

(Dated: 17 June 2022)

The crystallization of amorphous solids impacts fields ranging from inorganic crystal growth to biophysics. Promoting or inhibiting nanoscale epitaxial crystallization and selecting its final products underpins applications in cryopreservation, semiconductor devices, oxide electronics, quantum electronics, structural and functional ceramics, and advanced glasses. As precursors for crystallization, amorphous solids are distinguished from liquids and gases by the comparatively long relaxation times for perturbations of the mechanical stress and for variations in composition or bonding. These factors allow experimentally controllable parameters to influence crystallization processes and to drive materials towards specific outcomes. For example, amorphous precursors can be employed to form crystalline phases, such as polymorphs of Al_2O_3, VO_2, and other complex oxides, that are not readily accessible via crystallization from a liquid or through vapor-phase epitaxy. Crystallization of amorphous solids can further be guided to produce a desired polymorph, nanoscale shape, microstructure, and orientation of the resulting crystals. These effects can enable advances in applications in electronics, magnetic devices, optics, and catalysis. Directions for the future development of the chemical physics of crystallization from amorphous solids can be drawn from the impact of structurally complex and non-equilibrium atomic arrangements in liquids and the atomic-scale structure of liquid-solid interfaces.

[a)]Electronic mail: pgevans@wisc.edu

[b)]Electronic mail: schmidt@chem.wisc.edu

I. INTRODUCTION

Amorphous solids crystallize through atomic-level and nanoscale processes drawing on chemical, thermodynamic, mechanical, and nanostructural phenomena. Improving the current state of understanding and control of these processes promises to provide new ways to exploit the fundamental processes involved in crystallization. A key question in technological applications of materials synthesis is how to *guide* crystallization to form particular solids with desirable stable or metastable phases, selected orientations, or three-dimensional nanoscale geometries. Within this scope of potential outcomes, controlling the defect concentration, crystalline phase, and composition of epitaxy and crystal growth, in particular, remains an important challenge in many materials systems, including complex oxides, epitaxial and nanocrystalline semiconductors, and hybrid organic-inorganic perovskite semiconductors.[1] This perspective discusses aspects of crystallization from an amorphous phase in the solid state, a process affecting a wide range of materials. Semiconductors and complex oxides crystallize from the amorphous phase guided by a single-crystal substrate via solid-phase epitaxy (SPE).[2] In the biological sciences, metastable crystalline forms of solid materials have important roles in cryopreservation and biomineralization.[3,4] Atmospheric and planetary systems depend on crystallization processes involving amorphous solid water.[5–7] In all cases, the structure of interfaces, the kinetics of atomic and molecular rearrangement during crystallization, the valence of the component atoms, and the structure of the amorphous phase play important roles.

The scope of parameters of relevance to the crystallization of amorphous solids is illustrated in Fig. 1(a). These parameters include (i) the structure and nanoscale geometry of the substrate, which have a role in templating the crystallized layers, (ii) the polymorph, orientation and defect structure of the crystallized material, all of which can be distinct from the substrate, (iii) the composition of the crystallized material, and (iv) the atomic arrangement and bonding on both sides of the advancing amorphous-crystalline interface. Finally, there are the structural and chemical properties of the amorphous layer itself, such as the mechanical stress, composition, and structural perturbation due to nanoscale dimensionality. All of these parameters can potentially be employed to guide the epitaxial crystallization of amorphous materials from crystalline seeds.

This perspective illustrates the points that unify nanoscale mechanisms of crystallization across multiple amorphous materials. The overall goal is to provide an overview of ideas relevant to guiding crystallization and to point out commonalities among different materials. Two model systems

TABLE I. Factors affecting the nanoscale epitaxial crystallization of amorphous materials.

Factor	Selected References
Epitaxial template and amorphous/crystalline interface structure: bonding and substrate interface effects	8,9
Cation valence and phase selection depending on crystallization environment	10
Externally applied stress	9
Structure of the amorphous phase, structural relaxation	11–14
Competition between seeded and homogeneous nucleation	15–19
Density difference between amorphous and crystalline phases	20–23

are used here to illustrate the principles that can be employed to guide crystallization using the templating effects at interfaces and the structural, chemical, and ionic state of the amorphous solid. These systems are the crystallization of (i) amorphous solid water (ASW) to form crystalline ice, which is important in the context of biology, atmospheric science, and planetary science and (ii) structurally and compositionally complex metal oxides with wide-ranging applications in optics, electronics, and electromechanical technologies. The model systems have common features, including the roles of interfaces, variation of the structure of the amorphous phase as a function of preparation conditions and processing history, the development of mechanical stress, and the importance of nanoscale geometries. In each case, the final crystalline products can depend on the structure and history of the amorphous phase. The perspective concludes with directions in which the crystallization of amorphous materials can, in principle, be guided by phenomena that arise in the crystallization at liquid/solid interfaces but which are not yet exploited in the crystallization of amorphous solids. The factors that influence the amorphous-to-crystalline transition, along with examples of references to the effects of these factors are summarized in Table I.

Recent advances in theory, computation, synthesis, and characterization promise to provide new insights and improved control of crystallization processes. Computational approaches to understanding crystallization include molecular dynamics studies of the structure of amorphous solids and amorphous-crystalline interfaces and the kinetics of crystallization.[24,25] A key computational advance has involved the development of enhanced sampling techniques that bias molecular dy-

namics simulations towards rare events in crystallization and allow free-energy landscapes to be explored. The enhanced sampling approach has recently been applied to the crystallization of amorphous SiO_2, which would be prohibitively difficult to study in classical molecular dynamics simulations.[26] In experiments, recent developments in *in situ* transmission electron microscopy (TEM) provide insight into the phases formed during crystallization and the kinetics of oxide and ice crystallization.[27–29] The development of instrumentation employing the high brilliance of synchrotron x-ray sources allows nanoscale epitaxial crystallization to be probed *in situ*.[30–33] In bulk, synchrotron diffraction techniques have been adapted to discover the sequence of phases that forms during the crystallization of multi-component liquids.[34] Corresponding technological developments in nanoscale patterning provide nucleation sites for crystallization using nanotechnology, for example by synthesizing and transferring single-unit-cell-thick crystalline oxide sheets for patterning the surface of single crystals.[35,36]

The crystallization of amorphous solids is distinguished from crystal growth from a liquid or vapor in several ways. First, the processes relaxing structural or chemical perturbations in amorphous solids occur over long times in comparison with crystallization. The processes relaxing chemical or structural perturbations each involve atomic motions but are fundamentally distinct and thus diffusion, stress relaxation, crystal nucleation, and crystallization from an existing seed can occur with different rates and temperature dependence. The kinetics of structural rearrangement in amorphous solids are in general far slower than liquids.[37,38] The viscosity of liquid complex oxides at their melting point is typically in the range 1-100 mPa s. The viscosities of Al_2O_3 and $DyScO_3$ at their melting points, for example, are 2.72 and 49.86 mPa s, respectively.[39] As described in more detail below, the stress is relaxed on the Maxwell relaxation timescale set by the elastic constants and the viscosity. For oxide liquids this predicted time is on the order of 10^{-12} s or less, relaxing mechanical stress in the liquid over periods far shorter than the time required for crystallization. In amorphous solids, the relationship is the opposite. Because the relaxation of spatial variations of structural features within amorphous solids can occur at timescales far slower than crystallization, the structural, elastic, and composition variations persist during crystallization and influence the selection and formation of the final crystalline phase.

The time required for crystallization over a nanoscale distance d is d/v_{cryst}, where v_{cryst} is the crystallization velocity. Values of v_{cryst} range from 0.1 to 100 nm/min for $SrTiO_3$, $CaTiO_3$, Al_2O_3, and other oxides at temperatures ranging from approximately 300 to 800 °C.[15,40,41] The velocity typically exhibits an Arrhenius temperature dependence.[15,40,41] The crystallization of ASW also

occurs at rates within this range at a temperature of 128 K.[16] The temperature dependence of the crystallization time for d=5 nm is shown in Fig. 1(b) for $SrTiO_3$, a prototypical complex oxide, using the velocities and activation energy reported by Chen *et al.*[15]. The characteristic time for crystallization of $SrTiO_3$ at this length scale ranges from 10 s at 800 °C to 10^3 s at 300 °C.

The characteristic time for the relaxation of tensile viscoelastic stress is $\tau_{relax} = 3\eta/E$, where η is the viscosity and E is Young's modulus.[37] Similarly, the relaxation time for shear stress is η/G, where G is the shear modulus.[37] The example of amorphous SiO_2 illustrates the range of relaxation times that can be expected in oxides. The glass transition of SiO_2 is at 1885 °C.[42] At this temperature, the relaxation times of a hypothetical viscoelastic solid with E=100 GPa, approximately matching SiO_2 at viscosity $\eta = 10^{12}$ Pa s, yields a relaxation time on the order of 10 s. This mechanical relaxation time is thus already comparable to the timescale of crystallization at the glass transition temperature, and can be expected to increase exponentially at lower temperatures. More specific estimates provide insight into relaxation times in an experimentally relevant range of temperatures far below the melting point. The viscoelastic relaxation time for the prototypical complex oxide $SrTiO_3$ is shown in Fig. 1(b). The range of temperatures in Fig. 1(b) includes those at which crystallization from a seed can proceed for submicron distances without competing homogeneous nucleation.[15] As shown in Fig. 1(b), the viscoelastic relaxation time for $SrTiO_3$ ranges from 10^5 s at 800 °C to far longer times at lower temperatures.

Figure 1(b) also illustrates an important gap in the present state of knowledge of amorphous complex oxides in the temperature range of interest for deposition and crystallization. The crystallization rate and Young's modulus of $SrTiO_3$ are available in the literature for a range of deposition conditions, gas environments, and temperatures.[15,43,44] Viscosity measurements for amorphous complex oxides at temperatures on the order of 500 °C or less, relevant to crystallization, are not yet reported. The estimates of the viscoelastic relaxation time in Fig. 1(b) use the viscosity derived from mechanical measurements of polycrystalline crystallized $SrTiO_3$.[45] In the case of metallic glasses, there is evidence that the viscosity of amorphous materials far below the melting point depends on their thermal history and the degree of crystallization.[46] There is also some experimental evidence that the upper limit of the room-temperature viscosity of SiO_2 is on the order of 5×10^{17} Pa s, rather than continuing the very rapid scaling with temperature that is observed at elevated temperatures.[47] The uncertainty in the viscosity makes precise estimation of the viscoelastic relaxation times in the low-temperature range uncertain. In any event, even with this uncertainty, the these relaxation times within amorphous complex oxides are far longer than

the time required for crystallization. As such, the entire volume of nanoscale amorphous complex oxides would be expected to crystallize prior to significant viscoelastic relaxation.

The time required for diffusion of the cations in metal oxides over nanometer-scale distances is also, in general, far longer than the time required for the local (on the order of 1 nm or less) rearrangements that result in crystallization. Figure 1(b) shows characteristic times for the diffusion of metal and oxygen ions over a distance of 1 nm in $SrTiO_3$. As with the viscosity, measurements of the diffusion constant in this temperature regime are often indirect. The characteristic time for the equilibration of the ionic composition in Fig. 1(b) employs an effective diffusion constant for metal ions in $SrTiO_3$ drawn from an analysis of mechanical relaxation in crystalline $SrTiO_3$.[45] The time required to equilibrate oxygen concentrations in $SrTiO_3$ is reported from oxygen diffusion measurements and is far shorter than the metal-ion diffusion and crystallization time.[45] Diffusion can also be dramatically different between the crystalline amorphous phases of oxides and can, for example in $SrTi_{0.65}Fe_{0.35}O_{3-\delta}$, increase significantly upon crystallization.[48] Based on available estimates, it is evident from Fig. 1(b) that the distribution of metal ions is not smoothed by diffusion at the timescale associated with crystallization across a wide range of temperatures. The relatively slow rate of diffusion in comparison with crystallization simultaneously prevents separation of initially homogeneous amorphous layers into compositionally distinct phases by suppressing the required mass transport and also allows built-in compositional profiles to be maintained because inhomogeneity is not smoothed out by diffusion. Nanoscale gradients in the cation valence may be smoothed by oxygen diffusion and may not be preserved during crystallization. In $SrTiO_3$, crystallization of a 5 nm layer occurs before chemical composition equilibration or stress relaxation for all temperatures less than 1000 °C. The relative slowness of diffusion means that it is critical to assure that, in systems for which the targeted crystallized material has uniform composition, the amorphous precursor has the precise composition of the desired crystalline phase and is homogeneous on the nm-scale. The relative slowness of cation diffusion also means that cation transport is not be fast enough to yield phase separation or to smooth intentionally introduced composition profiles.

Similar considerations apply to the ASW. The low-temperature viscosity and elastic constants of ASW have been reported and give viscoelastic relaxation times that are long in comparison with the crystallization timescale. The viscosity of ice at the reported glass transition temperature, T_g=136 K, is 10^{12} Pa s.[6] The low-temperature shear modulus of amorphous ice is 1.2 GPa.[49] The resulting relaxation time η/G at 136 K is thus 900 s. An interesting point of difference

between ASW and oxide systems is that transformations in ASW occur at temperatures near the glass transition temperature, and thus can have shorter elastic relaxation times than in oxides. As discussed below, however, structural effects arising from elastic distortion are observed in the crystallization of ASW.[23] A slow mechanical relaxation time can thus be expected in many systems and leads to long-length-scale elastic effects in crystallization that arise due to mechanical stress. Relaxation and diffusion timescales in ASW are likely to be longer than crystallization times across a wide range of relevant conditions and materials.

The shapes of crystallized regions observed in low-dimensional crystallization in multiple different amorphous solid systems are similar, as shown in the micrographs Figs. 1(c)-(e). A depiction of the seeded lateral crystallization of $SrTiO_3$ within an amorphous $SrTiO_3$ thin film and the resulting crystal morphology are shown in Fig. 1(c).[50,52] $SrTiO_3$ and other complex oxides with the perovksite structure have applications in correlated electron phenomena, including in the realization of two-dimensional electron gases, piezoelectric materials, and transparent conductors formed by oxide crystallization.[10,53] Similar microstructuctural features result from the crystallization of $CaCO_3$, a process relevant to biomineralzation, as illustrated in Fig. 1(d).[51,54] A further electronic and optoelectronic application of nanoscale amorphous materials crystallization is in chalcogenide phase change materials, which is underpinned by the same principles and result in similar morphologies, as illustrated in Fig. 1(e).[21] The principles and processes governing crystallization yield crystalline morphologies for ASW with similar shapes and relative size distributions to those observed in oxide and chalcogenide systems. The TEM images in Fig. 1(f) show the nucleation and growth of ice nanocrystals during the heating of ASW for temperatures up to the completion of the transformation to polycrystalline ice at 156 K.[6]

II. ICE AND AMORPHOUS SOLID WATER

A. Relevance and applications of the crystallization of amorphous solid water

The crystallization of ASW exemplifies many of the ideas discussed above and provides a point of comparison (and, in some cases, contrast) with the related crystallization of amorphous oxides. ASW is most typically generated in experiments through vapor deposition onto a substrate held at low temperature on the order of tens of K.[5,55] Under such conditions, the deposited molecules lack sufficient mobility to relax into their crystalline lattice and are kinetic trapped in a non-equilibrium

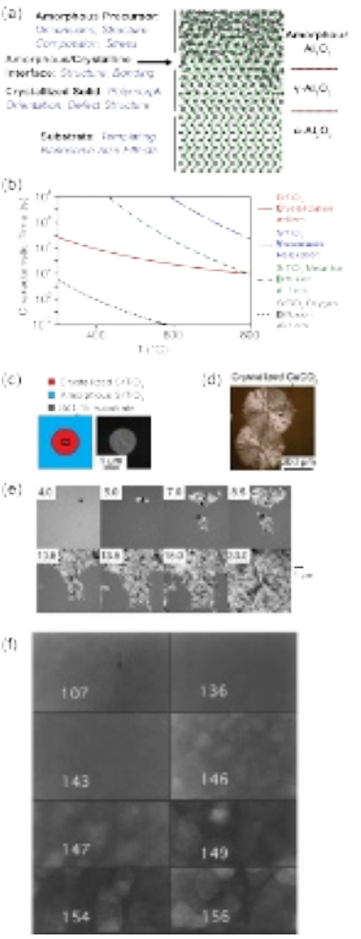

1.png

FIG. 1. (a) Nanoscale crystallization of amorphous solids involves phenomena and properties in the amorphous solid, the crystallized solid, at the interface between them, and in the crystalline substrate that serves as the structural template. Al_2O_3 graphic adapted with permission from Liu *et al.* [8]. Copyright 2020 American Chemical Society. (b) Timescales of crystallization over a distance of 5 nm, the viscoelastic stress relaxation, and diffusion of metal ions and oxygen over a distance of 1 nm for $SrTiO_3$. Parameters for these estimates are given in the text. (c) Schematic and scanning electron micrograph of the seeded nanoscale lateral crystallization of an amorphous $SrTiO_3$ thin film, after 840 min at 450 °C, after Marks *et al.* [50]. The open square indicates the location of a pre-deposited $SrTiO_3$ seed crystal. (d) Morphology resulting from crystallization of amorphous $CaCO_3$. Reprinted with permission from Pecher, Guenoun, and Chevallard [51]. Copyright 2009 American Chemical Society. (e) Crystallization of amorphous $Ge_6Sn_2Sb_2Te_{11}$ at 125 °C. Reprinted with permission from Koch *et al.* [21], Copyright 2018, with permission from Elsevier. Labels give the elapsed time in minutes since the start of crystallization. (f) Transmission electron microscopy images of the crystallization of amorphous ice during heating. Labels indicate the temperature in K at which each image was acquired, after Jenniskens and Blake [6]. Copyright American Astronomical Society. Reproduced with permission.

(amorphous) configuration. Water exhibits a number of distinct amorphous solid phases, i.e. it is typically considered to be polyamorphous.[13] These phases include low-density amorphous (LDA), high-density amorphous (HDA), and very high-density amorphous (VHDA) structures;[13] we use the shorthand ASW as an umbrella term for the solids of amorphous water, without regard to a specific amorphous structure. The amorphous structures have a local tetrahedral hydrogen-bonding configuration, with two hydrogen-bond donors and two acceptors on average, similar to liquid water but with with increasing occupancy of additional interstitial waters in the first coordination shell.[56] The initial crystalline phases reached from bulk forms of the various amorphous phases of ASW are depicted in Fig. 2 for a wide range of temperatures and pressures from 0 to 500 K and 0.1 to 10 GPa, with arrows showing the typical observed kinetic products of crystallization.[13] Different crystalline polymorphs of ice result from the crystallization of ASW, depending on the pressure, temperature, and initial amorphous phase.

ASW prepared by vapor deposition onto a cold substrate typically yields the LDA phase, while subjecting crystalline ice to high pressures (in excess of 1.6 GPa) at low temperatures results in collapse into the HDA phase.[55] The crystallization phenomena that follow the preparation of the sample can be quite complicated and can depend in detail on the thermal history. For example, upon heating at ambient pressure, the HDA phase relaxes to the higher-volume LDA phase,[55] and, with continued heating, crystallizes into the cubic phase of crystalline ice (I_c).[5] In other cases, the amorphous has been described as consisting of two structurally distinct phases, one LDA-like and a higher temperature "hyper-quenched" phase, whose relative prevalence can be altered by rapid transient annealing via a laser pulse.[57] The details of such complex crystallization behavior are not completely captured by the general kinetic pathways shown in Fig. 2. The temperature at which crystallization is observed during the heating of ASW is often near or above T_g, when the relaxation times are shorter and are comparable to the timescale for its crystallization to ice.[58] The crystallization behavior is consistent with the observation that, during crystallization, ASW exhibits tremendously enhanced translational diffusion, more than 10^6 times higher than the corresponding values in crystalline ice.[59] At lower temperature, below 238 K including temperatures near T_G, crystallization rates are largely diffusion-driven.[60] In this sense, ice contrasts with metal oxides, where annealing and crystallization often occurs at temperatures far below T_G. Although difficult to quantify, this observation may suggest that the multitude of diverse metastable phases found in ASW may be somewhat more difficult to stabilize in oxides.

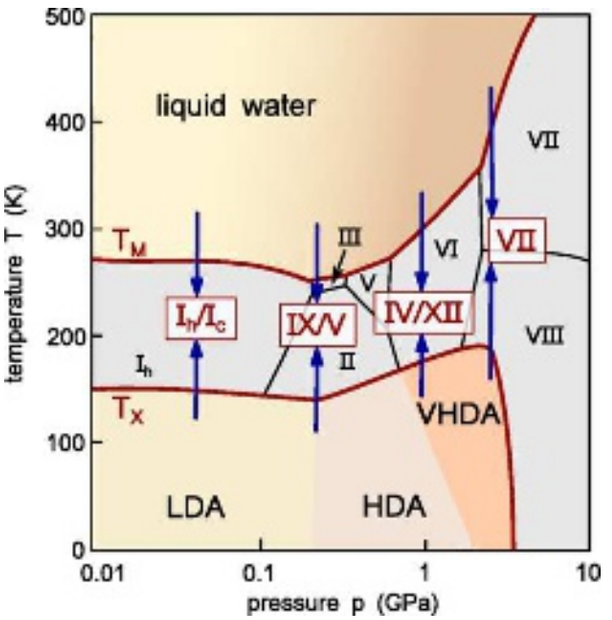

FIG. 2. Pressure and temperature dependence of the initial crystallized products resulting from heating or cooling of the various liquid, low-density amorphous (LDA), high-density amorphous (HDA), and very-high-density amorphous (VHDA) phases of water. Temperatures include the equilibrium melting point T_M and the (approximate) crystallization temperature T_X. The phases of ice are labeled with I_c, I_h, and numerals. Downward-pointing arrows indicate the initial, metastable crystallization products, labeled with numerals, of liquid water upon cooling. Upward arrows indicate the initial crystallization products of amorphous ices upon heating. Stable crystal phases are labeled in gray-colored regions in the background. Figure reprinted with permission from Amann-Winkel *et al.* [13]. Copyright 2016 by the American Physical Society.

B. Substrate effects in ASW crystallization phenomena

As is the case for other amorphous materials, the crystallization of ASW may proceed via homogeneous or heterogeneous nucleation. The competition between these nucleation pathways and the subsequent kinetics of crystal growth exhibit a sensitivity to the substrate onto which the ASW was deposited.[16–19] The role of the substrate in crystallization may be further explored by comparing ASW crystallization of thin films (where heterogeneous nucleation and subsequent crystal growth dominates) on different substrates, for example Pt(111) and crystalline ice (CI). As depicted in Fig. 3, the rate of crystallization of ASW increased by a factor of nearly 1000 when deposited on CI rather than Pt(111).[16] The apparent activation energy for crystallization is substantially lowered on the CI substrate.[16] In oxides, the activation energy for nucleation at sites

other than existing amorphous crystalline interfaces is higher than the activation energy for the motion of the amorphous/crystalline interface.[15]

The relative importance of the substrate on the nucleation of crystals within ASW depends on the ASW film thickness. As might be intuitively expected, the contribution due to crystal growth initiated at the substrate interface is reduced at larger ASW thicknesses. Homogeneous nucleation is thought to dominate in layers thicker than 100 monolayers (ML), which more closely resemble the bulk,[16,61] although the exact balance between homogeneous and heterogeneous nucleation is still somewhat debated.[62] For thinner films, the role of the substrate in the transformation kinetics becomes increasingly relevant. This competition between homogeneous an heterogeneous nucleation is also sensitively dependent on the structure of the substrate: whereas crystallization of ASW on epitaxial Pt(111) has often shown rapid growth from the Pt-ice interface, this heterogeneous nucleation is suppressed on non-epitaxial Pt(533) due to an inherently larger nucleation barrier.[63] In fact, for sufficiently thin films on Pt(533), nucleation at the ice-vacuum interface appears to dominate.[63] The results on Pt(533) are supported by other measurements which suggest that the nucleation rate at the ASW/vacuum interface exceeds that of bulk homogeneous nucleation in a film.[17]

The substrate-guided crystallization of ASW is reminiscent of SPE in oxides and semiconductor synthesis.[23,64] The crystallization mechanisms of ASW on CI and the SPE crystallization of semiconductors and oxides are similar in exhibiting a competition of homogeneous and heterogeneous nucleation and in the impact of the structure of the substrate structure on crystallization. In both cases, the sites of heterogeneous nucleation can include surfaces and interfaces. Experiments with thin-film CI substrates in which the temperature and ASW thickness are varied show that colder and thinner ASW layers films favor heterogeneous nucleation.[23] Lower temperatures correlate with lower homogeneous nucleation rates, thus favoring substrate-induced crystallization on CI. Similarly, thinner layers have a greater surface area per unit volume, thus favoring heterogeneous nucleation.[23] In addition to exhibiting a different regime of the competition between different nucleation mechanisms, thicker ASW films can crack as crystallization proceeds due to the elastic effects arising from the mismatch between the densities of ASW and crystalline ice.[23]

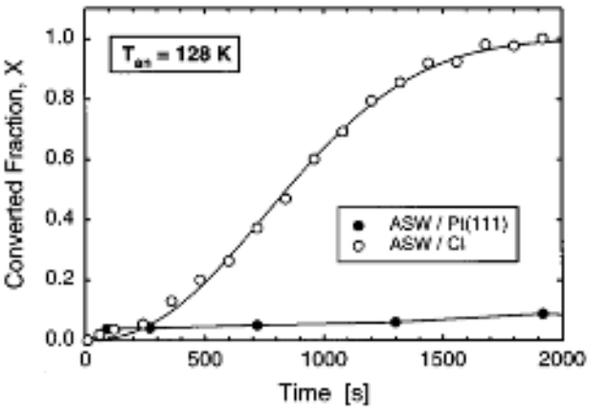

FIG. 3. Time dependence of the converted fractions of ASW layers on crystalline ice (CI) and Pt(111) during crystallization at annealing temperature T_{an} = 128 K, indicating the role of the CI substrate in promoting crystallization. Reprinted from Dohnálek *et al.* [16], with the permission of AIP Publishing.

C. Polymorph selection in ASW crystallization

The structure of ASW, even within a given amorphous phase, depends on the thermal history and evolves with temperature and the history of the material. The ASW structure, in addition to the substrate, can play an important role in determining the phases formed, morphology and crystal orientation, internal microstructure, and residual strain after crystallization. Crystallization of ASW typically yields cubic ice I_c. The formation of I_c is consistent with the prediction of classical nucleation theory (CNT), which favors the I_c phase because of the lower surface energy of cubic ice in comparison with the competing hexagonal phase (I_h).[6] Electron diffraction measurements show evolving characteristic peaks in ASW upon annealing, indicating that the structure becomes more similar to I_c.[5] The structural similarity provides one possible microscopic explanation for the lower interfacial energy of ASW with I_c. The amorphous structure thus appears to have an important role in determining the final product.

Certain ASW structures and specific sets of annealing conditions have a propensity to yield hexagonal I_h upon crystallization.[65] Seidl *et al.* [65] compared the results of crystallization of unannealed and expanded structural variants of HDA. Unannealed HDA (uHDA) is created by pressure-induced amorphization of crystalline ice I_h at low temperature, approximately 80K, which results in a heterogeneous macroscopic structure.[65,66]. uHDA yields a mixture of both ice I_c and I_h upon crystallization in contrast to predictions of CNT, which presumes a pure I_c final structure. This

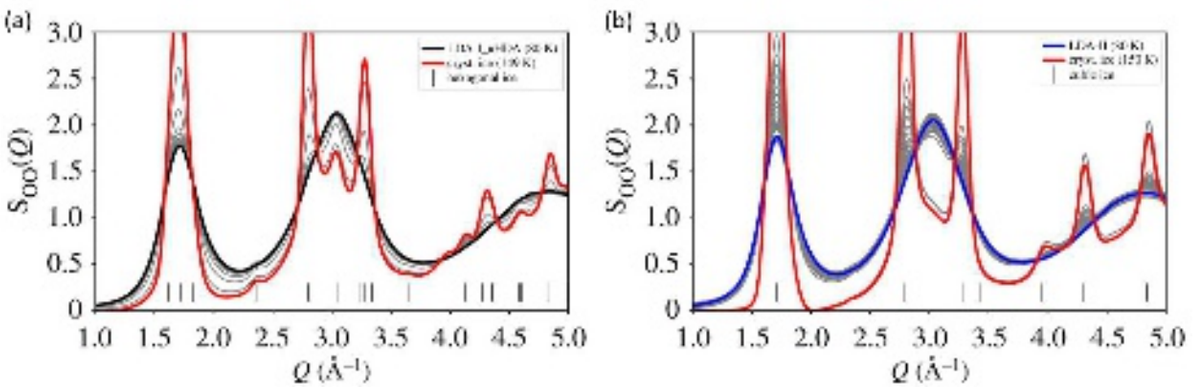

FIG. 4. Crystallization products upon annealing of two different ASW structures at 150 K, traced via the O−O structure factor $S_{OO}(Q)$ measured using x-ray scattering as a function of scattering wavevector Q. (a) Crystallizing LDA-I forms hexagonal I_h, while (b) LDA-II results in cubic I_c. Reproduced from Mariedahl *et al.* [14] with permission from the Royal Society of Chemistry.

difference may arise from residual features similar to parent ice I_h not fully removed by pressure-induced amorphization.[65] Expanded HDA (eHDA) is produced from uHDA by further heating and relaxation prior to crystallization. In contrast with uHDA, eHDA possesses a *homogeneous* structure and an expanded interplanar spacing of the lowest-angle x-ray reflection compared with uHDA.[67] Since all residual parent features present in uHDA from I_h have (presumably) been removed by thermal relaxation, eHDA yields exclusively I_c. A similar sensitivity to the initial ASW structure has been found for LDA. LDA with different preparations, and thus subtly different amorphous structures, yields either I_c or I_h.[14] These two forms, termed LDA-I and LDA-II, exhibit a structural difference observed by measuring the O-O structure factor over the course of crystallization, as shown in Fig. 4. The crystallization of LDA-I yields I_h, while LDA-II yields I_c crystals in which there exists a high degree of structural disorder. For both HDA and LDA, the underlying implication is that the structure of the amorphous phase can play a determining factor in the outcome of the crystallization. This influence can be due to residual common underlying structural motifs between amorphous and crystalline phases. Computational studies have probed the free-energy landscape for the formation of I_h and I_c.[68,69] Ice crystallization, has been further extended to explore both I_h and I_c polymorphs simultaneously.[70] Overall, studies of the crystallization of ASW benefit from advances in instrumentation, theory and computation, and by the exchange of key concepts with the crystallization of other amorphous materials.

III. PHASE SELECTION AND GEOMETRIC CONTROL IN CRYSTALLIZATION OF AMORPHOUS COMPLEX OXIDES

The crystallization of amorphous complex oxides involves phenomena arising from atomic scale bonding at interfaces, the nanoscale variation of strain, and the composition and valence of the ionic components. Epitaxial crystallization of complex oxides can be induced by a homoepitaxial or heteroepitaxial interfaces. Homoepitaxial or heteroepitaxial SPE can be induced in a wide range of oxides, including TiO_2, Al_2O_3, $SrTiO_3$.[15,35,71] Several factors influence the selection of the phase and orientation of the crystallized layer. Homoepitaxial Al_2O_3, for example, can adopt either the γ- or α-Al_2O_3 polymorphs depending on the the characteristics of the seed crystal.[71,72] Homoepitaxial crystallization via SPE on the two-dimensional surface of the c-plane α-Al_2O_3 substrate favors γ-Al_2O_3.[72] The selection of γ-Al_2O_3 as the initial phase upon crystallization appears to be influenced by comparatively small density difference between γ-Al_2O_3 and amorphous Al_2O_3, as well as by the continuity of the oxygen sublattice between γ-Al_2O_3 and the α-Al_2O_3 substrate.[8,73] Altering the geometry from planar to the three-dimensional structure associated with crystallization from nanoscale seed crystals can lead to the crystallization of α-Al_2O_3.[71] The difference may arise from the presentation of lateral (rather than vertical) crystal faces on the seed, because of the relative sizes of the seed and substrate, or because the configuration of the seed may lead to the presence of additional atomic steps at the amorphous/crystalline interface. More generally, the selection of the polymorph in Al_2O_3 can be linked to a combination of interface structural effects, stress effects due to the difference in density between the amorphous and crystalline forms, and the similarity of the crystalline and amorphous sublattice structures (e.g. oxygen arrangement).[8] In the case of the crystallization of ASW described above, the large density difference led to mesoscopic and macroscopic effects that included the development of cracks in the crystallized ice.[23] For oxides in general, the plastic deformation that arises in response to the density difference appears not to involve cracking but instead leads to the introduction of dislocations that cause the local crystal orientation to change continuously as the crystallization front advances laterally into the amorphous material.[20,36]

The energy landscape of the crystallization process for amorphous solids evolves as a function of temperature. The landscape can be studied via enhanced sampling techniques in molecular dynamics[74] from which free energy differences between the amorphous and crystallized phases can be extracted, as recently demonstrated for SiO_2,[26] calcite,[75] and ASW.[68,69] Further devel-

opment of computational techniques can reveal the temperature dependence of the free-energy landscapes of other oxides, including those for which multiple polymorphs can be nucleated, such as Al_2O_3. In principle, the variation of the landscape may result in the activation of different crystallization pathways at different temperatures.

Amorphous metal oxides share many of the structural motifs observed in their crystalline counterparts. The arrangements of metal-centered oxygen-bounded polyhedra in amorphous TiO_2 and Al_2O_3 are shown in Figs. 5(a) and (b), respectively. The crystallization of amorphous oxides at the amorphous-crystalline interface occurs through a change in the arrangement of these polyhedra. The rearrangement is reflected by a change in the geometric order parameters describing the arrangement and connection of the ions. The Steinhardt order parameter describes the connection of ions using an expansion in terms of spherical harmonics.[76] The correlations can include all ions, or oxygen-oxygen (O-O) or cation-cation coordination. For simulations of the crystallization of Al_2O_3 the $\bar{q}_6$ order parameter for Al-Al and O-O correlations is particularly useful in distinguishing amorphous Al_2O_3 from crystalline α-Al_2O_3. The Steinhardt order parameter plotted in Fig. 5(c) illustrates the structural differences between α-Al_2O_3 and amorphous Al_2O_3 after the simulated preparation of the amorphous layer and allows the amorphous-crystalline interface to be defined and tracked as the crystallization is simulated. Crystallization processes involve changes in these configurations at the amorphous/crystalline interface.[8]

A. Selection of the crystallized oxide phase

Several systems exhibit crystallization processes in which only a single final crystalline form is reasonably accessible after crystallization. Examples of such systems include Si, SiGe alloys, $SrTiO_3$, and $CaTiO_3$, for which no other crystalline polymorphs or compounds of different ionic valence appear during crystallization. Alloying or doping with impurities in these systems affects the rates of crystallization by changing both the amorphous-crystalline interface velocity and the activation energy that sets temperature dependence of the velocity. For example, the activation energy for crystallization in $SrTiO_3$ depends on the concentration of dissolved hydrogen.[44] Similarly, the crystallization of SiGe solid solutions results in the formation of an SiGe alloy with the diamond-cubic structure at a velocity that depends on the Si-Ge composition.[2] The dependence of the interface velocity on the Ge concentration arises from the variation of the interface attachment rate as a function of the local chemical environment, with a significantly slower attachment rate

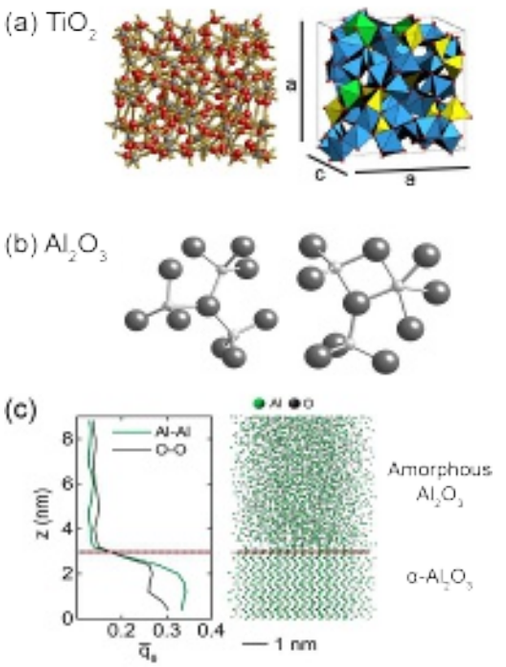

5.png

FIG. 5. (a) Atomic coordination (left) and structural building blocks (right) of amorphous TiO_2. Republished with permission of IOP Publishing Ltd. (all rights reserved), from Köhler *et al.*[77]; permission conveyed through Copyright Clearance Center, Inc. (b) Corner-sharing tetrahedra (left) and edge-sharing polyhedra (right) in amorphous Al_2O_3. Reprinted (figure) with permission from Gutiérrez and Johansson[25]. Copyright 2022 by the American Physical Society." (c) Steinhardt order parameter $\bar{q}_6$ for O-O and Al-Al arrangements (left) and the amorphous/crystalline α-Al_2O_3 interface (right). Reprinted with permission from Liu *et al.*[8]. Copyright 2020 American Chemical Society.

for Si in an Si-rich environment.[2] Beyond these systems, other metal oxides can be expected to exhibit additional compositional effects because of the multiple valences available for many metal ions and because multiple crystalline polymorphs can be produced.

The formation of amorphous layers with slight differences in composition can lead to the crystallization of different compounds in systems in which multiple crystalline phases are relevant to crystallization. The phases that form are particularly sensitive to the precursor composition in systems in which one or more of the components adopt multiple oxidation states. The Sr-V-O system shows this behavior, and complicates the development of $SrVO_3$ for use as a correlated-electron transparent conductor. This system exhibits multiple phases with a 1:1 Sr:V ratio but with different structures, O concentrations, and V valence.[78,79] Favoring the formation of $SrVO_3$ over other

crystalline phases involves promoting the stabilization of V^{4+} among oxidation states of V, which include V^{3+}, V^{4+}, and V^{5+} and combinations thereof. In vapor-phase epitaxial growth via molecular beam epitaxy the valence of V can be controlled by setting the oxygen partial pressures within a narrow growth window.[79] When formed via SPE $SrVO_3$ is favored by controlling the activity of O_2 during the deposition of the amorphous layer and crystallization.[10] This direction to the desired phase using the oxygen activity has also been demonstrated in a few other oxide systems. SPE of yttrium iron garnet (YIG) in an oxygen gas environment avoids the formation of a competing $YFeO_3$ phase.[80] Controlling the oxidizing environment allows the Delafossite electronic conductor $PtCoO_2$ to form without decomposition into metallic Pt.[81] The principle that the crystallized phase depends on the oxygen environment is also familiar from the synthesis and transformation of oxide single crystals, including $Ca_2Co_2O_5$.[82]

As in the case of the crystallization of ASW discussed above, there are indications that the atomic-scale structure of the of the amorphous oxides precursor affects the phase resulting from crystallization. In a particular example, the preparation of amorphous VO_2 influences the polymorph that is subsequently formed during crystallization.[11] The structure of amorphous VO_2 depends strongly on the repetition rate of the laser during pulsed-laser deposition (PLD), as shown in the x-ray scattering patterns and pair distribution functions in Fig. 6(a).[11] The rhombohedral R phase of VO_2 or a mixture of R and monoclinic M1 phases can form upon crystallization, depending on the laser repetition rate. It is an intriguing possibility that the observed difference in the structure of amorphous VO_2 formed at different laser repetition rates has a direct influence on the phase selected during crystallization. There are indications from computational studies of several oxides that the phase resulting from the relaxation of an initially randomized structure can exhibit different polymorphs depending on the initial conditions.[83]

A similar dependence of the crystallization behavior on the conditions for the preparation of the amorphous solid has been observed in TiO_2. The final crystallized form depends on factors that are varied during the preparation of TiO_2. First, the TiO_2 polymorph resulting from crystallization depends on the oxygen deficiency resulting from with the deposition conditions during sputtering and PLD.[84,85] The brookite polymorph of TiO_2 was formed under conditions in which the oxygen content was below the nominal TiO_2 stoichiometry.[84] In addition, Mangun *et al.* also speculate that residual stress resulting from the deposition process influences the phase selection.[84] Finally, higher deposition rates for amorphous TiO_2 thin films also favor the formation of the brookite and rutile phases over anatase.[85] The oxygen concentration between the two TiO_2 layers due to the

different deposition rates is apparent as a difference in the electrical resistivities of the amorphous TiO_2 layers.[85]

The structure of amorphous complex oxides evolves dynamically during crystallization. An example of this evolution is apparent in the x-ray scattering pattern of amorphous $SrTiO_3$, which becomes sharper and develops a higher peak intensity before crystallization, as shown in Fig. 6(b).[15] The evolution of the $SrTiO_3$ scattering pattern before crystallization may indicate that crystallization occurs after the onset of short-range atomic mobility within the amorphous phase. The rearrangement within the amorphous phase also leads to the development of mechanical stress before crystallization upon heating in amorphous $SrTiO_3$.[43] The structural changes in the amorphous phase before crystallization may represent local relaxation from a less stable structure produced by the deposition process. The stress that develops in this way is not relaxed through viscous flow over the timescales relevant to crystallization, consistent with the atomic scale of the rearrangement apparent in the x-ray scattering patterns in Fig. 6(b).[15] The scattered intensity from the amorphous layer occurs at an angle that is distinct from the x-ray reflections from the crystallized material. The angular profile of the scattered of the sharpens during heating and retains this shape during the initial growth of the crystalline phase.[15] A similar relationship between structural changes is apparent in the connection between molecular diffusion and crystallization is observed in ASW discussed above.[59] Beyond the dynamical evolution during heating, the structure of amorphous solids can be influenced by nanoscale size effects. The static structure of Al_2O_3 layers with few-nm thicknesses, where surface and interface effects are important, is different from thicker layers, with differences in the coordination of Al.[86] There is a possibility that these structural differences will affect crystallization.[86]

The interface bonding effects described above can cause the kinetics of crystallization to depend on the geometric orientation of the amorphous/crystalline interface. The velocity of the amorphous/crystalline interface during the crystallization of amorphous Si on a single-crystal Si substrate depends on the crystallographic orientation of the substrate.[9] In the case of complex oxides, the crystallization of velocity of $SrTiO_3$ is similar on (100) and (110) surfaces of $SrTiO_3$.[40] Crystallization on the (111) faces of $SrTiO_3$ is qualitatively different, with reports of complex time-dependent kinetics.[40] The orthorhombic perovskite $CaTiO_3$ similarly presents a more complex case than the (100) and (110) faces of $SrTiO_3$. The Crystallization velocities on the *a*- or *c*-axis oriented faces of $CaTiO_3$ exhibit a low activation energy and thus a higher low-temperature velocity in comparison with the *b*-axis oriented faces.[40] At the nanoscale, the orientation dependence

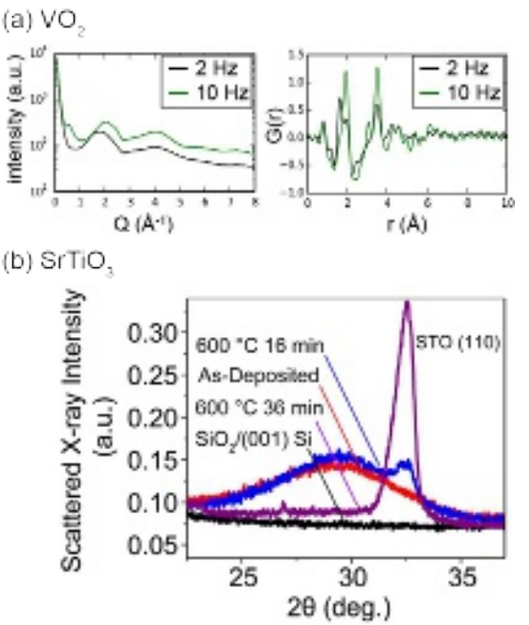

6.png

FIG. 6. (a) X-ray scattering patterns (left) and pair distribution functions (right) for amorphous VO_2 thin films deposited at different pulsed laser deposition laser repetition rates, after Stone *et al.*[11]. Licensed under a Creative Commons Attribution (CC BY) license (b) X-ray scattering patterns collected with an x-ray wavelength of 1.5406 Å exhibit structural differences in amorphous $SrTiO_3$ between the as-deposited form and before crystallization at 600 °C. Reprinted with permission from Chen *et al.*[15]. Copyright 2017 American Chemical Society. The time dependence of the intensity distribution near the amorphous intensity maximum in the range near 2θ=29°indicates that the structure of the amorphous phase evolves during heating. The (110) x-ray reflection of $SrTiO_3$ is labeled STO (110) and occurs at an different 2θ angle than scattering from the amorphous layer.

of the velocity of the amorphous/crystalline interface can result in faceting in some crystallized oxides, including TiO_2.[35]

Composition variations built into the creation of the amorphous material in order to permit the design of compositionally structured crystals. Composition are preserved throughout crystallization because the characteristic distance for ionic diffusion is significantly shorter than than the crystallization front displacement. An example of the incorporation of nanoscale composition variation in the crystallized material is apparent in the cross-sectional TEM image in Fig. 7(a). A 5 nm-thick layer of amorphous Al_2O_3 was formed at the interface between the $SrTiO_3$ substrate and a thicker amorphous $PrAlO_3$ layer as a result of the nucleation delay during atomic-layer

deposition.[12] The Al_2O_3 composition was preserved during crystallization at 750 °C and yielded a crystalline interface layer of γ-Al_2O_3.[12] The creation of composition profiles during deposition presents a route to the formation of epitaxial heterostructures.

B. Stress effects in nanoscale crystallization of complex oxides

Mechanical stress at the amorphous-crystalline interface affects the rate of crystallization because crystallization processes occur with an energy barrier that can be modified through a pressure (or more accurately stress tensor) that is described by an activation volume.[9] The product of the free-volume and stress tensors appears in thermal activation exponent, influencing the crystallization kinetics.[9] Stress arises from several sources: (i) the difference in the density of the amorphous and crystalline phases, (ii) the reconfiguration of the amorphous layer prior to crystallization, which increases the stress one particular case discussed below,[43], (iii) externally applied force, and (iv) mesoscopic effects arising from the multi-dimensional crystallization directions. At a slightly larger length scale, stress can lead to mesoscopic effects associated with stress-driven instabilities of the growth front. Morphological instabilities arise from the dependence of the crystallization velocity on the stress, including a coupling between the interface curvature and growth rate.[9,22]

In several cases, the longer-range distribution of stress leads to the formation of defects in the crystallized material that relax the mechanical stress. In crystallization over long distances in thin film layers, this relaxation of the stress can lead to a distinctive microstructure in which the continuous formation of defects leads to an overall position-dependent rotation of the orientation of the crystal.[20,36,87] This rotation does not arise in the crystallization of planar thin films because the volume difference can be accommodated by the displacement of the free surface. In lateral crystallization and other less-symmetric nanoscale geometries the movement of the surface is not sufficient to relax the stress. The generation of defects in the growing crystal yields rotations that can be on the order of several degrees per micron. A recent model for the distribution of dislocations resulting in the orientation rotation is shown in Fig. 7(b).[20] Similar rotational effects have been observed in GeO_2, SbS_3, and $SrTiO_3$.[20,36,87] The microstructure and orientational variation resulting from crystallization in these systems are shown schematically in Fig. 7(c) for the case of the crystallization of GeO_2.[20] The resulting spatial gradient of the orientation of the crystallized layer is also apparent in the x-ray microbeam diffraction study of SbS_3 shown in Fig.

7(d).[87] Interestingly, reports of lateral crystallization of the anatase form of TiO_2 do not describe the lattice rotation effect.[35] One possible explanation for the absence of apparent lattice rotation effects in TiO_2 is that, in both simulations and experiments under some deposition conditions, the density difference between amorphous TiO_2 and anatase on the order of 3% or less.[88,89] The density difference between amorphous and crystalline TiO_2 is thus smaller than the differences of more than 10% for $SrTiO_3$ and GeO_2 and could reduce the stress leading to the lattice rotation effect.[15,20] Strain remaining after crystallization can affect the structure and properties of the crystallized complex oxide, for example through the stabilization of a ferroelectric structure of $SrTiO_3$ by biaxial strain in epitaxial growth.[90]

IV. INSPIRATION FROM MATERIALS WITH COMPLEX LIQUID-PHASE STRUCTURES AND INTERFACE CONFIGURATIONS

The preceding sections show that there is a connection between the structure of amorphous materials, their interfaces with crystals, and the results of crystallization. Further inspiration for phenomena to be exploited in the future in crystallization of amorphous materials can be drawn from the structure and crystallization of liquids. The principles that relate the structure of amorphous materials and the products of crystallization are similar to those for the crystallization of liquids with complex structures. The structure and polymorph of the crystallized material can be influenced by the factors that affect the structure of the liquid phase. These are the composition, degree of undercooling, and the imprint of the symmetry of the crystalline interface structure onto the liquid. Similar factors have not yet been extensively exploited in the crystallization of amorphous solids. This comparison with solidification from liquids provides a frontier for future developments in the crystallization of amorphous solids.

A. Precrystallized structure in the liquid phase

Intermetallic compounds exhibit connections between the observed structure of liquids and their crystallization products,[91–94] akin to related ideas about the importance of local structure that have also been proposed in the nucleation of supercooled water.[4] Experimental and computational studies of liquids indicate that structural cues present in the precursor phase influence the formation of the final crystalline phase. The evidence points to the existence within the liquid

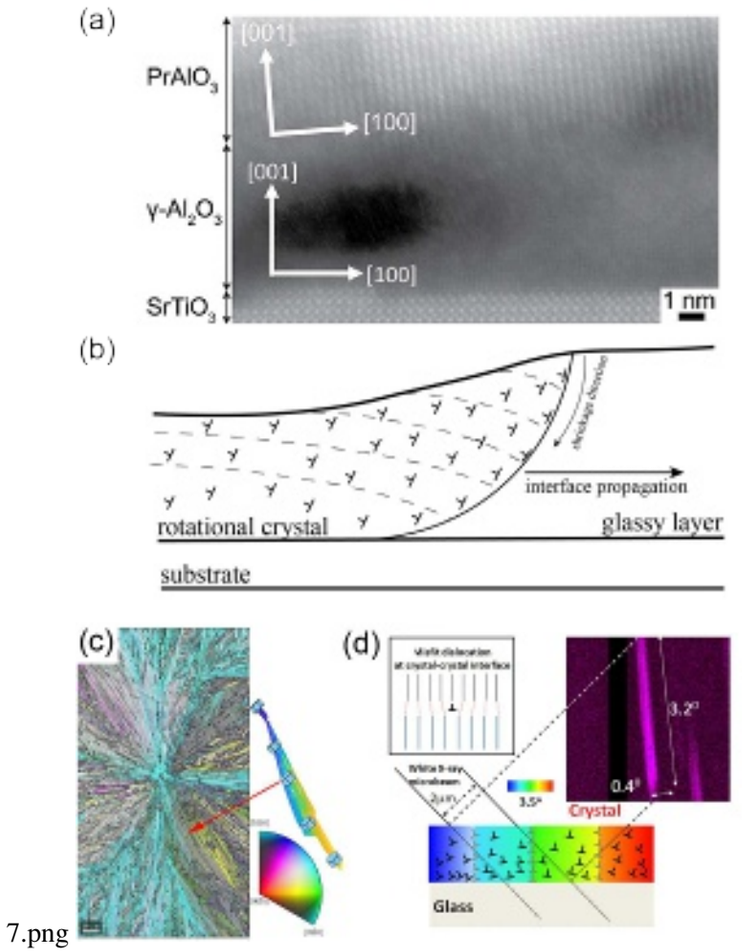

7.png

FIG. 7. (a) Preservation of the nanoscale composition distribution in a crystallized complex oxide. An Al_2O_3 layer with a thickness of 5 nm at the interface between $PrAlO_3$ and the $SrTiO_3$ substrate was retained after crystallization. Reprinted with permission from Waduge *et al.* [12]. Copyright 2019 American Chemical Society. (b) Model for the distribution of the defects arising during spherulitic crystallization of GeO_2, after Lutjes *et al.* [20]. Licensed under a Creative Commons Attribution (CC BY) license. (c) Distribution of crystallographic orientations resulting from the spherulitic crystallization of GeO_2, after Lutjes *et al.* [20]. Licensed under a Creative Commons Attribution (CC BY) license. (d) Model distribution of defects produced during the crystallization of SbS_3 on a glass substrate surface and the resulting elongation of the Laue x-ray reflection from that region, after Savytskii *et al.* [87]. Licensed under a Creative Commons Attribution (CC BY) license.

of clusters of the building blocks of the intermetallic phase.[92] In particular, the liquids employed in flux-mediated synthesis include clusters that are stabilized by the metal flux in configurations similar to their configuration in the crystal.[92] A particular example occurs in the Ba-Ge system. Cage-like structures of Ge around Ba atoms are form in the liquid state of Ba – Ge at melt compositions near the Ba-Ge eutectic at 17 atomic percent Ba, a structure that is similar to the $BaGe_{20}$ clusters in crystallized Ba_6Ge_{25} (16 atomic percent Ba) and Ba_8Ge_{43} (19 atomic percent Ba).[91] Other examples cited by Latturner[92] include Al_2Au clusters and $SiPd_9$ clusters.[93,94] Precrystalline structure with similarities to the crystallized phase, including in the octahedral configurations, is observed in simulations of the amorphous form of Ge-Sb-Te phase-change memory materials.[95–97] In an analogous case, sequencing the deposition of the components of the complex oxide $ScFeO_3$ during epitaxial growth from the vapor can produce a metastable layered polymorph.[98]

Simulations of the structure of the liquid form of intermetallic compounds and alloys allow the structural features of the liquid to be described more precisely. The spatial arrangement of clusters with different Frank-Kasper numbers, including icosahedral order and Z=9 and Z=10 configurations, in simulations of a PdSi liquid is shown in Fig. 8(a).[93] The statistical distribution of atoms among these configurations is a useful descriptor of order in crystalline phases and metallic glasses.[99–101] The Si-centered clusters in a Pd-Si liquid resemble the structure of the Pd-Si metallic glass and have been linked to the stabilization of Pd-Si glasses.[93] The pair distribution function constructed from *in situ* x-ray scattering studies probes the local structure of complex melts experimentally. The structure of the liquid melt is has been predicted to have an impact on the phases formed in crystallization of systems such as Cu-K-S for which the melt with excess K and S serves as a flux.[34,102,103] Drawing inspiration from this observation, it seems possible that a similar dependence of the structure of the amorphous solids or a persistent history dependence of the amorphous structure may lead to the nucleation of different solid phases.

The dependence of the structure of the liquid on its composition and on the temperature at which crystallization occurs can have a role in determining the structural phase of the material formed by crystallization. The polymorph of the ferroelectric $BaTiO_3$ formed during crystallization can be influenced by varying the supercooling of the liquid.[104] The cubic and hexagonal polymorphs of $BaTiO_3$ are selected at high (more than approximately 300 K) and low (less than approximately 180 K) values of the supercooling, respectively, as illustrated in the powder x-ray diffraction patterns in Fig. 8(c).[104] The cubic and hexagonal polymorphs of $BaTiO_3$ nucleate separately from the liquid phase, with nucleation rates that depend on the supercooling.[104] X-ray

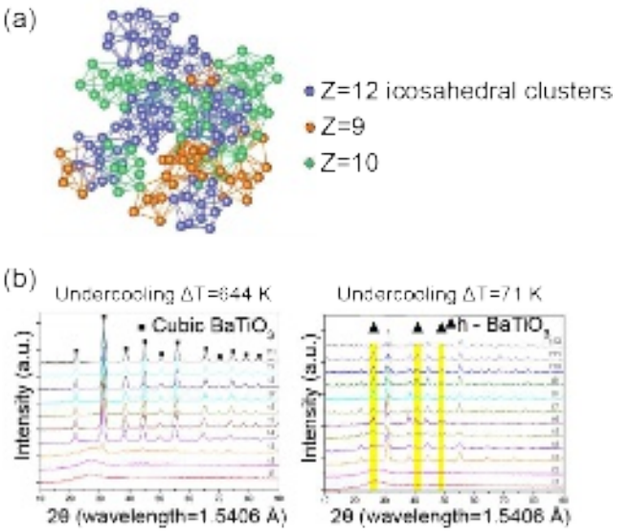

8.png

FIG. 8. (a) Clusters formed in simulations of Pd-Si liquids at 900 K, classified as local icosahedral order with Z=12 Frank-Kasper polyhedra, as well as order corresponding to Z=9 and Z=10 polyhedra. Reproduced from Dong *et al.* [93] with permission from the Royal Society of Chemistry. (b) Dependence of the crystalline phase formed from a $BaTiO_3$ melt, depending on the degree of undercooling. The degree of undercooling can select the formation of the tetragonal phase (left) or a mixture of tetragonal and hexagonal phases (right), after Ge *et al.* [104]. Licensed under a Creative Commons Attribution (CC BY) license.

scattering and molecular dynamics studies of the $BaTiO_3$ link the difference in nucleation of the two phases to temperature-dependent differences in the atomic coordination in the melt, including the degree of polymerization of TiO_4 polyhedra.[104]

The local configuration of ions in liquids can persist in a non-equilibrium distribution, depending on their processing history, and can affect the nucleation of solids. Potassium-sulfur melts exhibit structural similarity with the phases from which they are formed and can also have persistent non-equilibrated populations of sulfur chains of different lengths.[34,102,103] Chains of S within the K-S melt occur in different lengths with a distribution of populations that depend on the parent compounds.[34,102] Raman spectroscopy indicates that melts formed from K_2S_3 and K_2S_5 incorporated statistical distributions of ${S_n}^{2-}$ chains with $n = 3$ and $n = 5$ that were not in equilibrium with ${S_{n+1}}^{2-}$ and other chain lengths at 400 °C.[34,102] The observation of non-equilibrium structure within the melts points to the possibility that the crystallization can be selectively changed by changing the processing history of the amorphous material.

B. Interface structure imprinted on precursor phase

Insights into how the structure of the amorphous/crystalline interface can be further employed to influence crystallization can be gained from the role of the structure of liquid/crystalline interface in liquid crystallization. The liquid-phase effects described above point to new directions for using interfacial effects in amorphous crystallization, including exploiting the packing and coordination of an atomic-scale layer of the liquid near the interface.[105] The interface structure affects thermodynamic parameters of the interface, including the entropy and internal energy density. A diagram and sketch of thermodynamic quantities at the melting point T_M is shown in Fig. 9(a). The schematic in Fig. 9 likely simplifies the structural description, including the potential development of order arising from ionic charges. The order imparted by the formation of the interface, however, is likely in general to lead to a region of intermediate entropy between the entropy of the crystal S_C and the entropy of the liquid S_L. The entropy difference ΔS between the solid and liquid phases is reduced at the interface. The internal energy density U also differs between the two phases. In the model illustrated in Fig. 9(a), the reduction of entropy in the region near the interface corresponds to the interface free energy, or surface tension, σ.[105] There may also be an enthalpic contribution due to the interface, in addition to the entropy component illustrated in Fig. 9. The interfacial structure and interface energy in amorphous/crystalline interfaces are not yet completely explored but may have similar features and may affect crystallization. In addition to the oxide bonding and epitaxy issues discussed in the context of oxide crystallization above, there is an intriguing possibility that the complex oxide amorphous layers may exhibit structural order extending into the amorphous layer.

Two examples highlight the role of the liquid structure at the liquid-solid interface in crystallization and point to ways to employ similar concepts at the amorphous-solid interface during the crystallization amorphous solids. There are atomic-scale signatures of order in Al at the interface between liquid-Al and Al_2O_3, as shown in Fig. 9(b).[106] This order can have a role in subsequent crystal growth, for examples when the permeation of ambient oxygen to the interface leads to the formation of additional Al_2O_3.[106] The crystallization of liquid Au-Si at the eutectic composition on an Si (111) substrate involves an undercooling that depends on the structure of the interface.[107] The formation of the Au-induced Si (111) 6×6 reconstruction, as in Fig. 9(c) stabilizes 5-fold coordination in the liquid, and reduces the rate of the nucleation of the solid phase.[107] There are similar observations of ordering at the liquid Al/sapphire interface.[108] The further development of

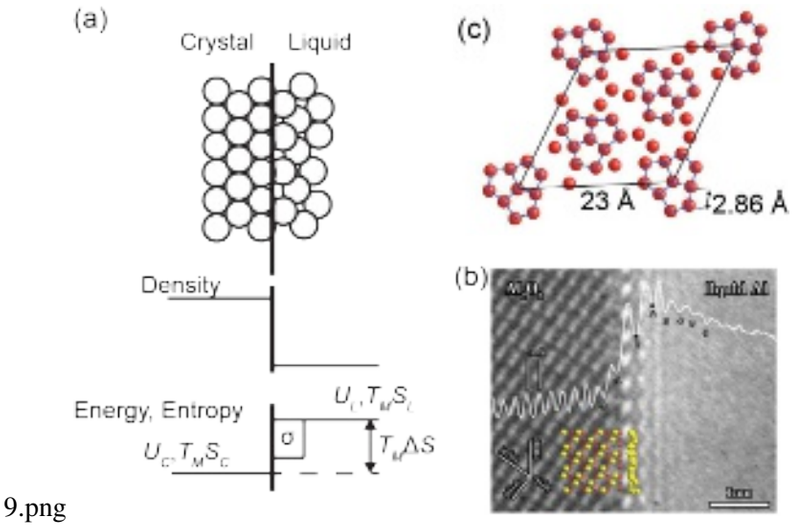

9.png

FIG. 9. (a) Structure, density, entropy S, entropy difference ΔS, internal energy U, and interface free energy or surface tension σ of a liquid/crystal interface at the melting temperature T_M. Reprinted from Spaepen [105] with permission from Elsevier. (b) Ordering of Al at the interface between liquid Al and crystalline Al_2O_3, from Oh *et al.* [106]. Reprinted with permission from AAAS (c) Locations of Au atoms in the Au-induced Si (111) 6×6 reconstruction, which promotes 5-fold order in the Au-Si eutectic liquid. Adapted by permission from Springer Nature from Schülli *et al.* [107].

in situ x-ray scattering and TEM techniques can enable the exploration of similar effects in the crystallization of oxides and ASW.

In the areas described in this section, the connection between the structure and processing history of liquids and their crystallization products is more completely developed than the analogous phenomena in the crystallization of amorphous materials. The liquid/solid interface thus provides possible perspectives for the future direction of efforts to guide amorphous crystallization.

V. CONCLUSIONS

The crystallization of amorphous materials provides valuable routes to the synthesis of materials, to control crystallization in biological systems, and in understanding the state of water in atmospheric and planetary science. The crystallization of amorphous water is also essential in biological applications including cryopreservation of cells and tissue.[109] Other biologically relevant systems depend on the nanoscale crystallization of amorphous oxides including $CaCO_3$.[51,54]

Several experimental factors influence the rate and phase of crystal growth during the crystal-

lization process, including factors such as interface structure, externally applied stress, and cation valence, that can be experimentally controlled. Ultimately controlling these factors is essential in guiding crystallization. The same factors also provide the means to envision new forms of crystalline materials, including phases that are challenging to stabilize with other synthesis approaches, three-dimensional epitaxial forms, and nanostructures with novel microstuctures. The factors apply across the range of complex oxide materials and in the crystallization of amorphous solid water, as discussed here.

Similar concepts apply across several materials, as illustrated here in particular for water and metal oxides. The understanding and eventual control of these processes have the potential to enable the crystallization of novel phases and the formation of heterostructures and other nanomaterials. Specific areas of impact include the crystallization of specific polymorphs, including metastable polymorphs, the use of structural cues to promote, guide, or suppress crystallization and crystallization that preserves structure imparted into the amorphous precursor. Although not considered explicitly in this perspective, there is an extensive literature in the non-epitaxial devitrification of covalent-network glasses in the bulk and in the crystallization of compounds dissolved in glasses that employs similar concepts.[110] Further advances in the field of amorphous crystallization will draw on concepts from bulk and interface structure of liquids.

ACKNOWLEDGMENTS

This research was primarily supported by NSF through the University of Wisconsin Materials Research Science and Engineering Center (DMR-1720415). T.D.J. acknowledges support from the National Science Foundation Graduate Research Fellowship under Grant No. DGE-1747503. T.D.J. also acknowledges the support provided by the Graduate School and the Office of the Vice Chancellor for Research and Graduate Education at the University of Wisconsin-Madison with funding from the Wisconsin Alumni Research Foundation.

REFERENCES

[1]J. L. MacManus-Driscoll, M. P. Wells, C. Yun, J.-W. Lee, C.-B. Eom, and D. G. Schlom, "New approaches for achieving more perfect transition metal oxide thin films," APL Mater. **8**, 040904 (2020).

[2]T. E. Haynes, M. J. Antonell, C. A. Lee, and K. Jones, "Composition dependence of solid-phase epitaxy in silicon-germanium alloys - experiment and theory," Phys. Rev. B **51**, 7762–7771 (1995).

[3]J. M. Campbell, F. C. Meldrum, and H. K. Christenson, "Is ice nucleation from supercooled water insensitive to surface roughness?" J. Phys. Chem. C **119**, 1164–1169 (2015).

[4]P. Gallo, K. Amann-Winkel, C. A. Angell, M. A. Anisimov, F. Caupin, C. Chakravarty, E. Lascaris, T. Loerting, A. Z. Panagiotopoulos, J. Russo, J. A. Sellberg, H. E. Stanley, H. Tanaka, C. Vega, L. Xu, and L. G. M. Pettersson, "Water: A Tale of Two Liquids," Chem. Rev. **116**, 7463–7500 (2016).

[5]P. Jenniskens and D. F. Blake, "Structural transitions in amorphous water ice and astrophysical implications," Science **265**, 753–756 (1994).

[6]P. Jenniskens and D. F. Blake, "Crystallization of amorphous water ice in the solar system," Astrophys. J. **473**, 1104–1113 (1996).

[7]A. Hudait and V. Molinero, "What determines the ice polymorph in clouds?" J. Am. Chem. Soc. **138**, 8958–8967 (2016).

[8]R. Liu, O. Elleuch, Z. Wan, P. Zuo, T. D. Janicki, A. D. Alfieri, S. E. Babcock, D. E. Savage, J. R. Schmidt, P. G. Evans, and T. F. Kuech, "Phase Selection and Structure of Low-Defect-Density γ-Al_2O_3 Created by Epitaxial Crystallization of Amorphous Al_2O_3," ACS Appl. Mater. Interfaces **12**, 57598–57608 (2020).

[9]W. Barvosa-Carter, M. Aziz, A. Phan, T. Kaplan, and L. Gray, "Interfacial roughening during solid phase epitaxy: Interaction of dopant, stress, and anisotropy effects," J. Appl. Phys. **96**, 5462–5468 (2004).

[10]S. D. Marks, L. Lin, P. Zuo, P. J. Strohbeen, R. Jacobs, D. Du, J. R. Waldvogel, R. Liu, D. E. Savage, J. H. Booske, J. K. Kawasaki, S. E. Babcock, D. Morgan, and P. G. Evans, "Solid-phase epitaxial growth of the correlated-electron transparent conducting oxide $SrVO_3$," Phys. Rev. Mater. **5**, 083402 (2021).

[11]K. H. Stone, L. T. Schelhas, L. M. Garten, B. Shyam, A. Mehta, P. F. Ndione, D. S. Ginley, and M. F. Toney, "Influence of amorphous structure on polymorphism in vanadia," APL Mater. **4**, 076103 (2016).

[12]W. L. I. Waduge, Y. Chen, P. Zuo, N. Jayakodiarachchi, T. F. Kuech, S. E. Babcock, P. G. Evans, and C. H. Winter, "Solid-phase epitaxy of perovskite high dielectric $PrAlO_3$ films grown by atomic layer deposition for use in two-dimensional electronics and memory devices," ACS

Appl. Nano Mater. **2**, 7449–7458 (2019).

[13]K. Amann-Winkel, R. Böhmer, F. Fujara, C. Gainaru, B. Geil, and T. Loerting, "Colloquium: Water's controversial glass transitions," Rev. Mod. Phys. **88**, 011002 (2016).

[14]D. Mariedahl, F. Perakis, A. Späh, H. Pathak, K. H. Kim, C. Benmore, A. Nilsson, and K. Amann-Winkel, "X-ray studies of the transformation from high- to low-density amorphous water," Phil. Trans. Roy. Soc. A: Math. Phys. Eng. Sci. **377**, 20180164 (2019).

[15]Y. Chen, M. H. Yusuf, Y. Guan, R. B. Jacobson, M. G. Lagally, S. E. Babcock, T. F. Kuech, and P. G. Evans, "Distinct Nucleation and Growth Kinetics of Amorphous $SrTiO_3$ on (001) $SrTiO_3$ and SiO_2/Si: A Step toward New Architectures," ACS Appl. Mater. Interfaces **9**, 41034–41042 (2017).

[16]Z. Dohnálek, R. L. Ciolli, G. A. Kimmel, K. P. Stevenson, R. S. Smith, and B. D. Kay, "Substrate induced crystallization of amorphous solid water at low temperatures," J. Chem. Phys. **110**, 5489–5492 (1999).

[17]R. S. Smith, C. Yuan, N. G. Petrik, G. A. Kimmel, and B. D. Kay, "Crystallization growth rates and front propagation in amorphous solid water films," J. Chem. Phys. **150**, 214703 (2019).

[18]M. B. Davies, M. Fitzner, and A. Michaelides, "Routes to cubic ice through heterogeneous nucleation," Proc. Natl. Acad. Sci. USA **118**, e202524511832 (2021).

[19]L. Lupi, A. Hudait, and V. Molinero, "Heterogeneous Nucleation of Ice on Carbon Surfaces," J. Am. Chem. Soc. **136**, 3156–3164 (2014).

[20]N. R. Lutjes, S. Zhou, J. Antoja-Lleonart, B. Noheda, and V. Ocelik, "Spherulitic and rotational crystal growth of quartz thin films," Sci. Rep. **11**, 14888 (2021).

[21]C. Koch, T. Dankwort, A.-L. Hansen, M. Esters, D. Haeussler, H. Volker, A. von Hoegen, M. Wuttig, D. C. Johnson, W. Bensch, and L. Kienle, "Investigation of the phase change mechanism of $Ge_6Sn_2Sb_2Te_{11}$," Acta Mater. **152**, 278–287 (2018).

[22]A. Phan, T. Kaplan, L. Gray, D. Adalsteinsson, J. Sethian, W. Barvosa-Carter, and M. Aziz, "Modelling a growth instability in a stressed solid," Model. Sim. Mater. Sci. Eng. **9**, 309–325 (2001).

[23]Z. Dohnálek, G. A. Kimmel, R. L. Ciolli, K. P. Stevenson, R. S. Smith, and B. D. Kay, "The effect of the underlying substrate on the crystallization kinetics of dense amorphous solid water films," J. Chem. Phys. **112**, 5932–5941 (2000).

[24]N. Bernstein, M. J. Aziz, and E. Kaxiras, "Amorphous-crystal interface in silicon: A tight-binding simulation," Phys. Rev. B **58**, 4579–4583 (1998).

[25]G. Gutiérrez and B. Johansson, "Molecular dynamics study of structural properties of amorphous Al_2O_3," Phys. Rev. B **65**, 104202 (2002).

[26]H. Niu, P. M. Piaggi, M. Invernizzi, and M. Parrinello, "Molecular dynamics simulations of liquid silica crystallization," Proc. Natl. Acad. Sci. **115**, 5348–5352 (2018).

[27]A. R. Akbashev, G. Chen, and J. E. Spanier, "A Facile Route for Producing Single-Crystalline Epitaxial Perovskite Oxide Thin Films," Nano Lett. **14**, 44–49 (2014).

[28]S. Jesse, Q. He, A. R. Lupini, D. N. Leonard, M. P. Oxley, O. Ovchinnikov, R. R. Unocic, A. Tselev, M. Fuentes-Cabrera, B. G. Sumpter, S. J. Pennycook, S. V. Kalinin, and A. Y. Borisevich, "Atomic-Level Sculpting of Crystalline Oxides: Toward Bulk Nanofabrication with Single Atomic Plane Precision," Small **11**, 5895–5900 (2015).

[29]K. Tai, Y. Liu, and S. J. Dillon, "In Situ Cryogenic Transmission Electron Microscopy for Characterizing the Evolution of Solidifying Water Ice in Colloidal Systems," Microscop. Microanal. **20**, 330–337 (2014).

[30]G. Eres, C. M. Rouleau, Q. Lu, Z. Zhang, E. Benda, H. N. Lee, J. Z. Tischler, and D. D. Fong, "Experimental setup combining in situ hard x-ray photoelectron spectroscopy and real-time surface x-ray diffraction for characterizing atomic and electronic structure evolution during complex oxide heterostructure growth," Rev. Sci. Instrum. **90**, 093902 (2019).

[31]R. L. Headrick, J. G. Ulbrandt, P. Myint, J. Wan, Y. Li, A. Fluerasu, Y. Zhang, L. Wiegart, and K. F. Ludwig, Jr., "Coherent x-ray measurement of step-flow propagation during growth on polycrystalline thin film surfaces," Nature Commun. **10**, 2638 (2019).

[32]R. Liu, J. G. Ulbrandt, H.-C. Hsing, A. Gura, B. Bein, A. Sun, C. Pan, G. Bertino, A. Lai, K. Cheng, E. Doyle, K. Evans-Lutterodt, R. L. Headrick, and M. Dawber, "Role of ferroelectric polarization during growth of highly strained ferroelectric materials," Nature Commun. **11**, 2630 (2020).

[33]S. D. Marks, P. Quan, R. Liu, M. J. Highland, H. Zhou, T. F. Kuech, G. B. Stephenson, and P. G. Evans, "Instrument for in situ hard x-ray nanobeam characterization during epitaxial crystallization and materials transformations," Rev. Sci. Instrum. **92**, 023908 (2021).

[34]L. Soderholm and J. F. Mitchell, "Perspective: Toward "synthesis by design": Exploring atomic correlations during inorganic materials synthesis," APL Mater. **4**, 053212 (2016).

[35]K. Taira, Y. Hirose, S. Nakao, N. Yamada, T. Kogure, T. Shibata, T. Sasaki, and T. Hasegawa, "Lateral Solid-Phase Epitaxy of Oxide Thin Films on Glass Substrate Seeded with Oxide Nanosheets," ACS Nano **8**, 6145–6150 (2014).

[36]R. Liu, D. Sri Gyan, P. Zuo, S. D. Marks, D. E. Savage, T. Zhou, Z. Cai, M. Holt, S. Butun, S. Lu, N. Basit, S. E. Babcock, T. F. Kuech, and P. G. Evans, "Solid-phase epitaxial lateral overgrowth of rotating lattice complex oxides," in preparation (2022).

[37]A. H. Cottrell, *The Mechanical Properties of Matter* (Wiley, New York, 1964) pp. 194–199.

[38]R. B. Bird, W. E. Stewart, and E. N. Lightfoot, *Transport Phenomena* (Wiley, New York, 2002) p. 245.

[39]N. Crnogorac and H. Wilke, "Measurement of physical properties of $DyScO_3$ melt," Cryst. Res. Technol. **44**, 581–589 (2009).

[40]C. W. White, L. A. Boatner, P. S. Sklad, C. J. McHargue, J. Rankin, G. C. Farlow, and M. J. Aziz, "Ion-implantation and annealing of crystalline oxides and ceramic materials," Nucl. Instrum. Meth. Phys. Res. B **32**, 11–22 (1988).

[41]J. Jang, D. Yang, D. Moon, D. Choi, H. J. Lim, S.-G. Kang, D. Bae, H. N. Han, Y. Park, and E. Yoon, "Solid-phase epitaxy of a cavity-shaped amorphous alumina nanomembrane structure on a sapphire substrate," J. Cryst. Growth **498**, 130–136 (2018).

[42]R. H. Doremus, "Viscosity of silica," J. Appl. Phys. **92**, 7619–7629 (2002).

[43]D. J. Prakash, Y. Chen, M. L. Debasu, D. E. Savage, C. Tangpatjaroen, C. F. Deneke, A. Malachias, A. D. Alfieri, O. Elleuch, K. Lekhal, I. Szlufarska, P. G. Evans, and F. Cavallo, "Reconfiguration of amorphous complex oxides: A route to a broad range of assembly phenomena, hybrid materials, and novel functionalities," Small **18**, 2105424 (2021).

[44]T. W. Simpson, I. V. Mitchell, J. C. McCallum, and L. A. Boatner, "Hydrogen catalyzed crystallization of strontium titanate," J. Appl. Phys. **76**, 2711–2718 (1994).

[45]S. Webb, I. Jackson, and J. Fitz Gerald, "Viscoelasticity of the titanate perovskites $CaTiO_3$ and $SrTiO_3$ at high temperature," Phys. Earth Planet. Inter. **115**, 259–291 (1999).

[46]G. Wang, I. Jackson, J. Fitz Gerald, J. Shen, and Z. Stachurski, "Rheology and nanocrystallization of a $Zr_{41.25}Ti_{13.75}Ni_{10}Cu_{12.5}Be_{22.5}$ bulk metallic glass," J. Non-Cryst. Solids **354**, 1575–1581 (2008).

[47]M. Vannoni, A. Sordini, and G. Molesini, "Relaxation time and viscosity of fused silica glass at room temperature," Europ. Phys. J. E **34**, 92 (2011).

[48]H. B. Buckner, Q. Ma, J. Simpson-Gomez, E. J. Skiba, and N. H. Perry, "Multi-scale chemo-mechanical evolution during crystallization of mixed conducting $SrTi_{0.65}Fe_{0.35}O_{3-\delta}$ films and correlation to electrical conductivity," J. Mater. Chem. A **10**, 2421–2433 (2022).

[49]J. Hessinger, B. White, and R. Pohl, "Elastic properties of amorphous and crystalline ice films,"

Planet. Space Sci. **44**, 937–944 (1996).

[50]S. D. Marks, R. Liu, Y. Chen, Q. Li, S. J. Leake, D. E. Savage, S. E. Babcock, T. U. Schülli, and P. G. Evans, "Crystallographic rotation during solid-phase epitaxy of $SrTiO_3$ from nanoscale seed crystals," submitted (2022).

[51]J. Pecher, P. Guenoun, and C. Chevallard, "Crystalline calcium carbonate thin film formation through interfacial growth and crystallization of amorphous microdomains," Cryst. Growth. Des. **9**, 1306–1311 (2009).

[52]Y. Chen, J. A. Tilka, Y. Ahn, J. Park, A. Pateras, T. Zhou, D. E. Savage, I. McNulty, M. V. Holt, D. M. Paskiewicz, D. D. Fong, T. F. Kuech, and P. G. Evans, "Seeded Lateral Solid-Phase Crystallization of the Perovskite Oxide $SrTiO_3$," J. Phys. Chem. C **123**, 7447–7456 (2019).

[53]P. P. Aurino, A. Kalabukhov, N. Tuzla, E. Olsson, A. Klein, P. Erhart, Y. A. Boikov, I. T. Serenkov, V. I. Sakharov, T. Claeson, and D. Winkler, "Reversible metal-insulator transition of ar-irradiated $LaAlO_3/SrTiO_3$ interfaces," Phys. Rev. B **92**, 155130 (2015).

[54]Z. Liu, Z. Zhang, Z. Wang, B. Jin, D. Li, J. Tao, R. Tang, and J. J. De Yoreo, "Shape-preserving amorphous-to-crystalline transformation of $CaCO_3$ revealed by in situ TEM," Proc. Natl. Acad. Sci. **117**, 3397–3404 (2020).

[55]C. A. Angell, "Amorphous water," Ann. Rev. Phys. Chem. **55**, 559–583 (2004).

[56]J. L. Finney, D. T. Bowron, A. K. Soper, T. Loerting, E. Mayer, and A. Hallbrucker, "Structure of a New Dense Amorphous Ice," Phys. Rev. Lett. **89**, 205503 (2002).

[57]L. Kringle, W. A. Thornley, B. D. Kay, and G. A. Kimmel, "Reversible structural transformations in supercooled liquid water from 135 to 245 K," Science **369**, 1490–1493 (2020), arXiv:1912.06676.

[58]E. B. Moore and V. Molinero, "Ice crystallization in water's "no-man's land"," J. Chem. Phys. **132**, 244504 (2010).

[59]R. S. Smith, C. Huang, and B. D. Kay, "Evidence for molecular translational diffusion during the crystallization of amorphous solid water," J. Phys. Chem. B **101**, 6123–6126 (1997).

[60]Y. Xu, N. G. Petrik, R. S. Smith, B. D. Kay, and G. A. Kimmel, "Growth rate of crystalline ice and the diffusivity of supercooled water from 126 to 262 k," Proc. Natl. Acad. Sci. **113**, 14921–14925 (2016).

[61]P. Löfgren, P. Ahlström, J. Lausma, B. Kasemo, and D. Chakarov, "Crystallization kinetics of thin amorphous water films on surfaces," Langmuir **19**, 265–274 (2003).

[62]K. Harada, T. Sugimoto, F. Kato, K. Watanabe, and Y. Matsumoto, "Thickness dependent

homogeneous crystallization of ultrathin amorphous solid water films," Phys. Chem. Chem. Phys. **22**, 1963–1973 (2020).

[63]E. H. Backus, M. L. Grecea, A. W. Kleyn, and M. Bonn, "Surface crystallization of amorphous solid water," Phys. Rev. Lett. **92**, 236101 (2004).

[64]E. P. Donovan, F. Spaepen, D. Turnbull, J. M. Poate, and D. C. Jacobson, "Heat of crystallization and melting point of amorphous silicon," Appl. Phys. Lett. **42**, 698–700 (1983).

[65]M. Seidl, K. Amann-Winkel, P. H. Handle, G. Zifferer, and T. Loerting, "From parallel to single crystallization kinetics in high-density amorphous ice," Phys. Rev. B **88**, 174105 (2013).

[66]Y. Suzuki and Y. Tominaga, "Polarized raman spectroscopic study of relaxed high density amorphous ices under pressure," J. Chem. Phys. **133**, 164508 (2010).

[67]R. J. Nelmes, J. S. Loveday, T. Strässle, C. L. Bull, M. Guthrie, G. Hamel, and S. Klotz, "Annealed high-density amorphous ice under pressure," Nature Phys. **2**, 414–418 (2006).

[68]P. M. Piaggi and R. Car, "Phase equilibrium of liquid water and hexagonal ice from enhanced sampling molecular dynamics simulations," J. Chem. Phys. **152**, 204116 (2020).

[69]D. Quigley and P. M. Rodger, "Metadynamics simulations of ice nucleation and growth," J. Chem. Phys. **128** (2008).

[70]F. Giberti, M. Salvalaglio, and M. Parrinello, "Metadynamics studies of crystal nucleation," IUCrJ **2**, 256–266 (2015).

[71]H. Maret, D. Weisberg, H. M. Chan, and N. C. Strandwitz, "Seeded Solid-Phase Epitaxy of Atomic Layer Deposited Aluminum Oxide," Cryst. Growth Des. **16**, 1662–1666 (2016).

[72]J. C. McCallum, T. W. Simpson, and I. V. Mitchell, "Time-resolved reflectivity measurements of the amorphous-to-gamma and gamma-to-alpha phase-transitions in ion-implanted Al_2O_3," Nucl. Inst. Meth. Phys. Res. B **91**, 60–62 (1994).

[73]D. R. Clarke, "Epitaxial phase transformations in aluminum oxide," Phys. Status Solidi A - Appl. Mater. Sci. **166**, 183–196 (1998).

[74]G. C. Sosso, J. Chen, S. J. Cox, M. Fitzner, P. Pedevilla, A. Zen, and A. Michaelides, "Crystal Nucleation in Liquids: Open Questions and Future Challenges in Molecular Dynamics Simulations," Chem. Rev. **116**, 7078–7116 (2016).

[75]D. Quigley, P. M. Rodger, C. L. Freeman, J. H. Harding, and D. M. Duffy, "Metadynamics simulations of calcite crystallization on self-assembled monolayers," J. Chem. Phys. **131**, 094703 (2009).

[76]W. Lechner and C. Dellago, "Accurate determination of crystal structures based on averaged

local bond order parameters," J. Chem. Phys. **129**, 114707 (2008).

[77]T. Köhler, M. Turowski, H. Ehlers, M. Landmann, D. Ristau, and T. Frauenheim, "Computational approach for structure design and prediction of optical properties in amorphous TiO_2 thin-film coatings," J. Phys. D: Appl. Phys. **46**, 325302 (2013).

[78]J. C. Bouloux, J. Galy, and P. Hagenmul, "Ternary-Systems $MoMO-V_2O_5-VO_2$ (M=Ca, Sr, Ba)," Rev. Chim. Miner. **11**, 48–70 (1974).

[79]M. Brahlek, L. Zhang, C. Eaton, H.-T. Zhang, and R. Engel-Herbert, "Accessing a growth window for $SrVO_3$ thin films," Appl. Phys. Lett. **107**, 143108 (2015).

[80]P. Jang, S. Yamamoto, and H. Kuniki, "Growth of YIG films by solid phase epitaxy and their properties," Phys. Status Solidi A - Appl. Mater. Sci. **201**, 1851–1854 (2004).

[81]D. J. Hagen, J. Yoon, H. Zhang, B. Kalkofen, M. Silinskas, F. Börrnert, H. Han, and S. S. P. Parkin, "Atomic layer deposition of the conductive delafossite $PtCoO_2$," Adv. Mater. Interfaces **9**, 2200013 (2022).

[82]J. Zhang, H. Zheng, C. D. Malliakas, J. M. Allred, Y. Ren, Q. Li, T.-H. Han, and J. F. Mitchell, "Brownmillerite $Ca_2Co_2O_5$: Synthesis, stability, and re-entrant single crystal to single crystal structural transitions," Chem. Mater. **26**, 7172–7182 (2014).

[83]V. Stevanović, "Sampling polymorphs of ionic solids using random superlattices," Phys. Rev. Lett. **116**, 075503 (2016).

[84]J. S. Mangum, L. M. Garten, D. S. Ginley, and B. P. Gorman, "Utilizing TiO_2 amorphous precursors for polymorph selection: An in situ TEM study of phase formation and kinetics," J. Am. Ceram. Soc. **103**, 2899–2907 (2020).

[85]O. Agirseven, D. T. Rivella, J. E. S. Haggerty, P. O. Berry, K. Diffendaffer, A. Patterson, J. Kreb, J. S. Mangum, B. P. Gorman, J. D. Perkins, B. R. Chen, L. T. Schelhas, and J. Tate, "Crystallization of TiO_2 polymorphs from RF-sputtered, amorphous thin-film precursors," AIP Adv. **10** (2020).

[86]S. K. Lee and C. W. Ahn, "Probing of 2 dimensional confinement-induced structural transitions in amorphous oxide thin film," Sci. Rep. **4**, 4200 (2014).

[87]D. Savytskii, H. Jain, N. Tamura, and V. Dierolf, "Rotating lattice single crystal architecture on the surface of glass," Sci. Rep. **6**, 36449 (2016).

[88]B. D. Piercy, C. Z. Leng, and M. D. Losego, "Variation in the density, optical polarizabilities, and crystallinity of TiO_2 thin films deposited via atomic layer deposition from 38 to 150 °c using the titanium tetrachloride-water reaction," J. Vac. Sci. Technol. A **35** (2017).

[89]B. Prasai, B. Cai, M. K. Underwood, J. P. Lewis, and D. A. Drabold, "Properties of amorphous and crystalline titanium dioxide from first principles," J. Mater. Sci. **47**, 7515–7521 (2012).

[90]J. Haeni, P. Irvin, W. Chang, R. Uecker, P. Reiche, Y. Li, S. Choudhury, W. Tian, M. Hawley, B. Craigo, A. Tagantsev, X. Pan, S. Streiffer, L. Chen, S. Kirchoefer, J. Levy, and D. Schlom, "Room-temperature ferroelectricity in strained $SrTiO_3$," Nature **430**, 758–761 (2004).

[91]A. Ishikura, A. Mizuno, M. Watanabe, T. Masaki, T. Ishikawa, and S. Kohara, "Structure analysis of molten Ba-Ge alloys using electrostatic levitation technique combined with high-energy X-ray diffraction," J. Am. Ceram. Soc. **90**, 738–741 (2007).

[92]S. E. Latturner, "Clusters, assemble: Growth of intermetallic compounds from metal flux reactions," Acc. Chem. Res. **51**, 40–48 (2018).

[93]F. Dong, G. Q. Yue, Y. R. Guo, C. Qiao, Z. Y. Wang, Y. X. Zheng, R. J. Zhang, Y. Sun, W. S. Su, M. J. Kramer, S. Y. Wang, C. Z. Wang, K. M. Ho, and L. Y. Chen, "Si-centered capped trigonal prism ordering in liquid $Pd_{82}Si_{18}$ alloy study by first-principles calculations," RSC Adv. **7**, 18093–18098 (2017).

[94]L. H. Xiong, H. B. Lou, X. D. Wang, T. T. Debela, Q. P. Cao, D. X. Zhang, S. Y. Wang, C. Z. Wang, and J. Z. Jiang, "Evolution of local atomic structure during solidification of Al_2Au liquid: An *ab initio* study," Acta Mater. **68**, 1–8 (2014).

[95]J. Hegedus and S. R. Elliott, "Microscopic origin of the fast crystallization ability of ge-sb-te phase-change memory materials," Nature Mater. **7**, 399–405 (2008).

[96]A. Hirata, T. Ichitsubo, P. F. Guan, T. Fujita, and M. W. Chen, "Distortion of local atomic structures in amorphous ge-sb-te phase change materials," Phys. Rev. Lett. **120** (2018).

[97]S. Mukhopadhyay, J. Sun, A. Subedi, T. Siegrist, and D. J. Singh, "Competing covalent and ionic bonding in ge-sb-te phase change materials," Sci. Rep. **6** (2016).

[98]L. M. Garten, Z. Jiang, H. Paik, J. D. Perkins, A. Kakekhani, R. Fei, D. J. Werder, M. E. Holtz, D. S. Ginley, A. M. Rappe, D. G. Schlom, and M. L. Staruch, "Stromataxic stabilization of a metastable layered $ScFeO_3$ polymorph," Chem. Mater. **33**, 7423–7431 (2021).

[99]F. C. Frank and J. S. Kasper, "Complex alloy structures regarded as sphere packings. I. Definitions and basic principles," Acta Cryst. **11**, 184–190 (1958).

[100]F. C. Frank and J. S. Kasper, "Complex alloy structures regarded as sphere packings. II. Analysis and classification of representative structures," Acta Cryst. **12**, 483–499 (1959).

[101]D. R. Nelson, "Liquids and glasses in spaces of incommensurate curvature," Phys. Rev. Lett. **50**, 982–985 (1983).

[102]D. P. Shoemaker, Y.-J. Hu, D. Y. Chung, G. J. Halder, P. J. Chupas, L. Soderholm, J. F. Mitchell, and M. G. Kanatzidis, "In situ studies of a platform for metastable inorganic crystal growth and materials discovery," Proc. Natl. Acad. Sci. **111**, 10922–10927 (2014).

[103]D. P. Shoemaker, D. Y. Chung, J. F. Mitchell, T. H. Bray, L. Soderholm, P. J. Chupas, and M. G. Kanatzidis, "Understanding Fluxes as Media for Directed Synthesis: In Situ Local Structure of Molten Potassium Polysulfides," J. Am. Chem. Soc. **134**, 9456–9463 (2012).

[104]X. Ge, Q. Hu, F. Yang, J. Xu, Y. Han, P. Lai, J. Qin, and J. Li, "Anomalous structure transition in undercooled melt regulates polymorphic selection in barium titanate crystallization," Comm. Chem. **4**, 27 (2021).

[105]F. Spaepen, "A structural model for the solid-liquid interface in monatomic systems," Acta Met. **23**, 729–743 (1975).

[106]S. H. Oh, Y. Kauffmann, C. Scheu, W. D. Kaplan, and M. Rühle, "Ordered liquid aluminum at the interface with sapphire," Science **310**, 661–663 (2005).

[107]T. U. Schülli, R. Daudin, G. Renaud, A. Vaysset, O. Geaymond, and A. Pasturel, "Substrate-enhanced supercooling in AuSi eutectic droplets," Nature **464**, 1174 (2010).

[108]S. Ma, A. J. Brown, R. Yan, R. L. Davidchack, P. B. Howes, C. Nicklin, Q. Zhai, T. Jing, and H. Dong, "Atomistics of pre-nucleation layering of liquid metals at the interface with poor nucleants," Commun. Chem. **2**, 1 (2019).

[109]Y. Akiyama, M. Shinose, H. Watanabe, S. Yamada, and Y. Kanda, "Cryoprotectant-free cryopreservation of mammalian cells by superflash freezing," Proc. Natl. Acad. Sci. **116**, 7738–7743 (2019).

[110]T. Komatsu, "Design and control of crystallization in oxide glasses," J. Non-Cryst. Solids **428**, 156–175 (2015).

(a)

Amorphous Precursor: *Dimensions, Structure, Composition, Stress*

Amorphous/Crystalline Interface: *Structure, Bonding*

Crystallized Solid: *Polymorph, Orientation, Defect Structure*

Substrate: *Templating, Nanoscale Size Effects*

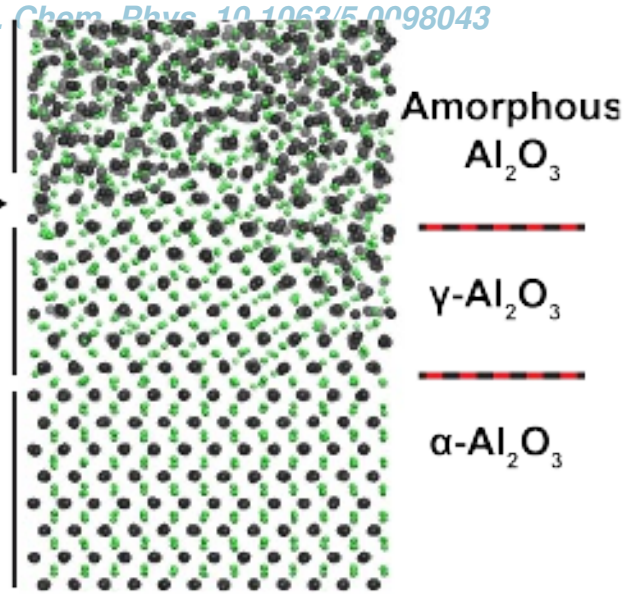

(b)

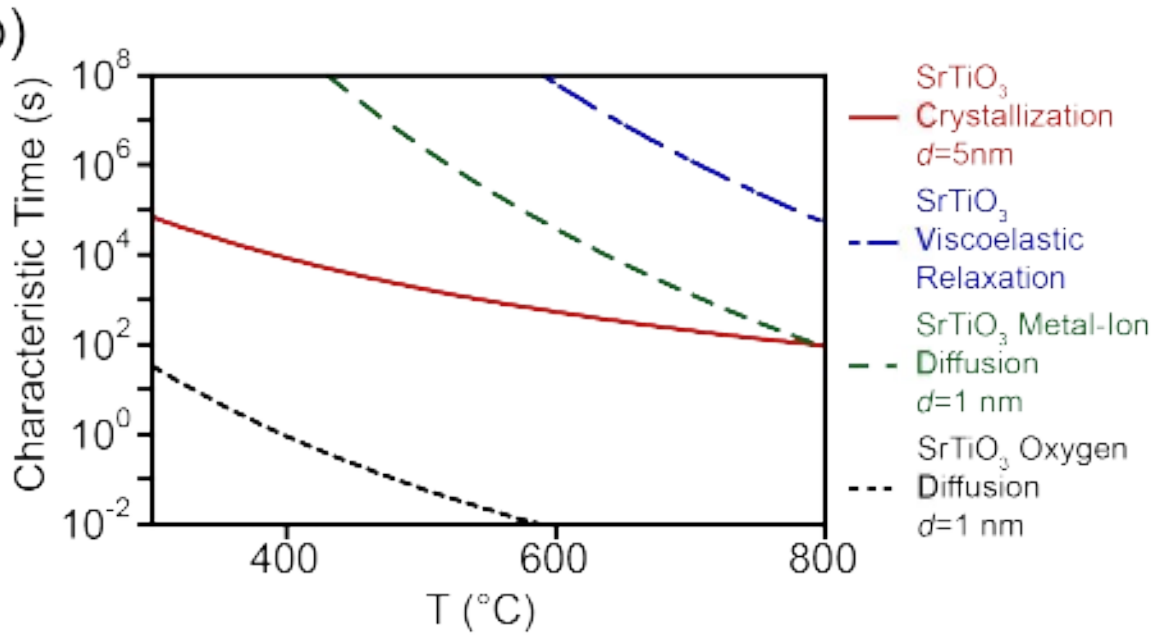

(c)

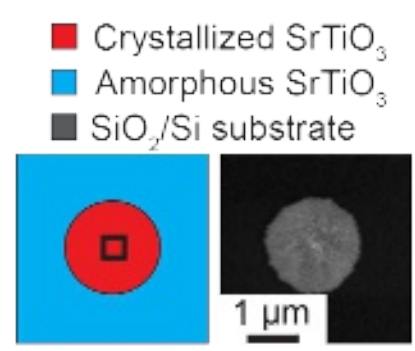

(d)

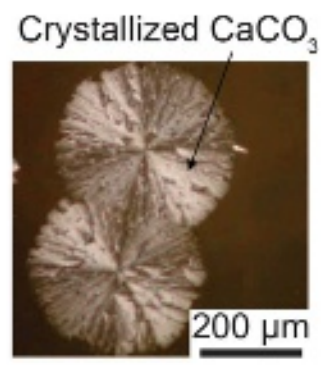

(e)

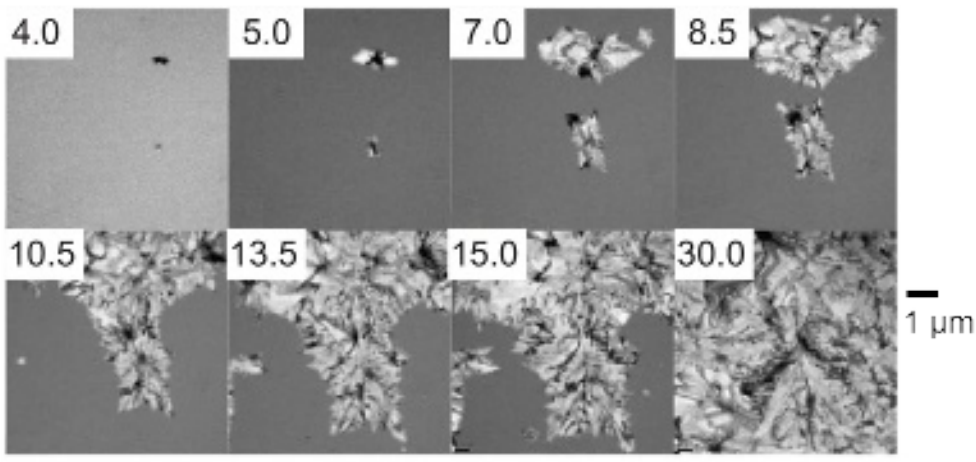

(f)

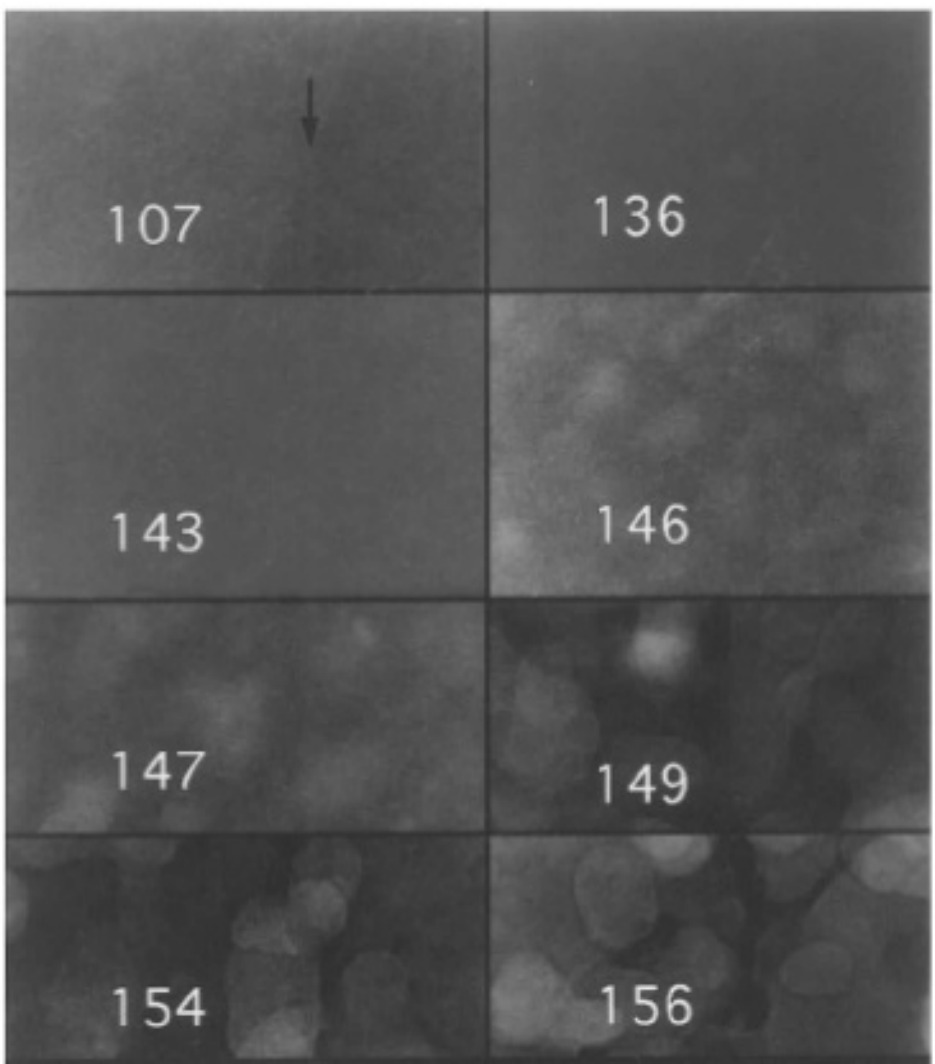

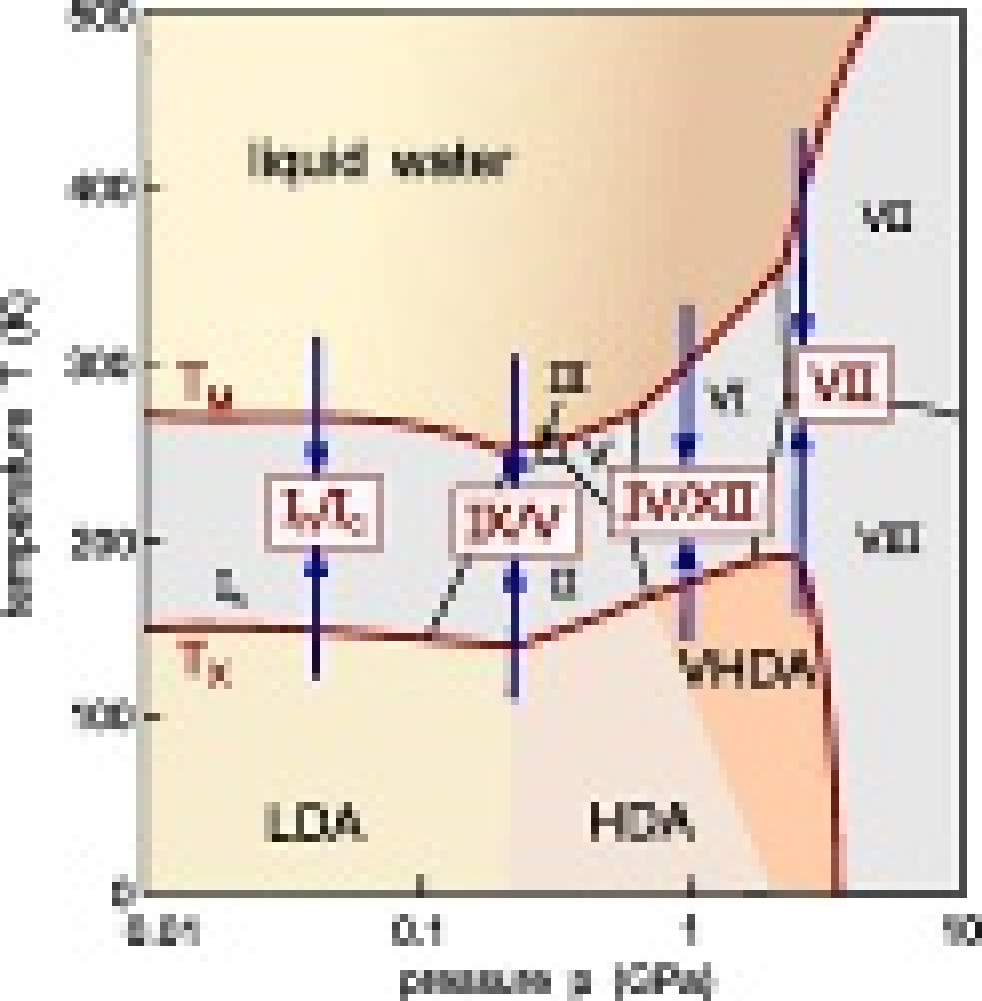
liquid water
VII
VI
III
V
VII
VIII
T_M
T_X
T_c
I$_h$
I/I$_c$
IX/V
IV/XII
II
VHDA
LDA
HDA
temperature T (K)
pressure p (GPa)

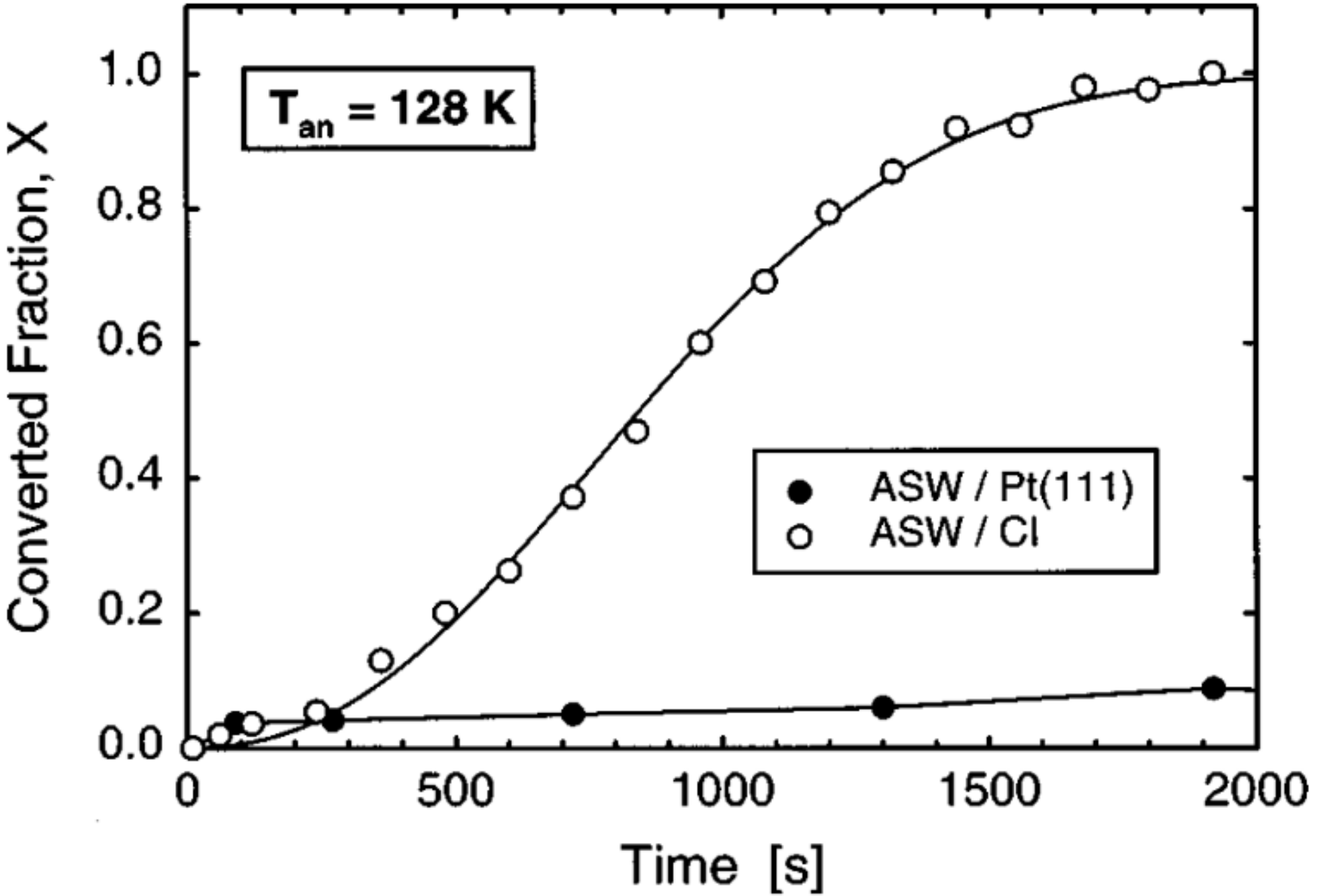
T_{an} = 128 K
ASW / Pt(111)
ASW / Cl
Converted Fraction, X
Time [s]
0.0
0.2
0.4
0.6
0.8
1.0
0
500
1000
1500
2000

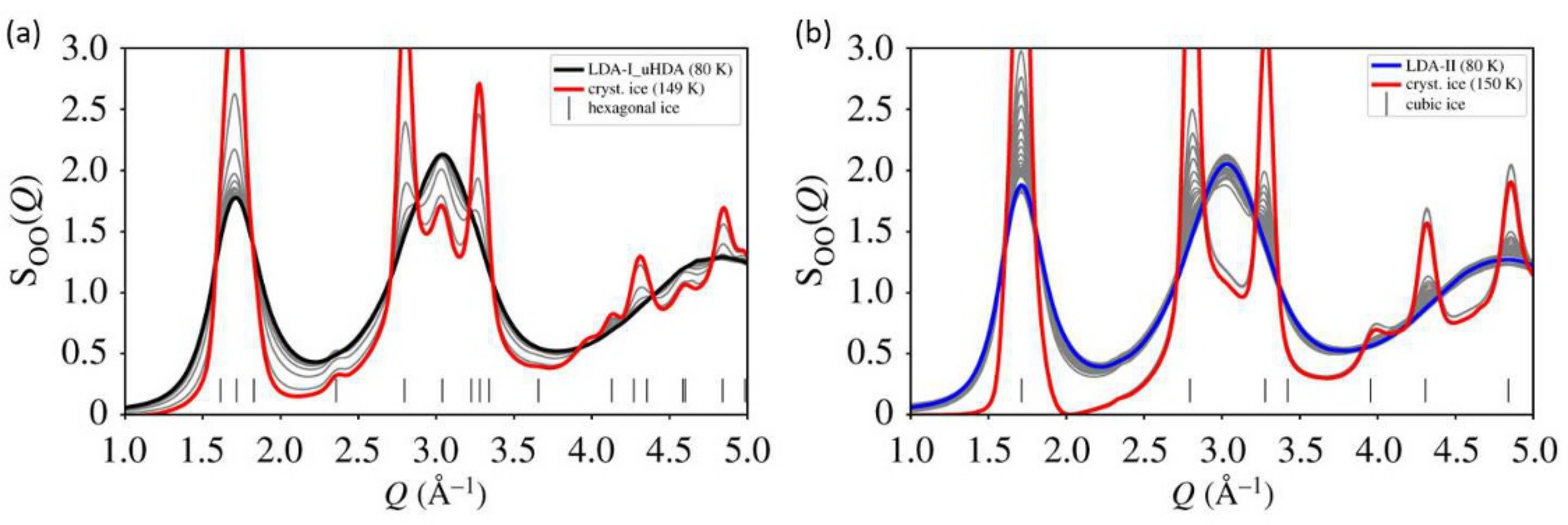
(a)
LDA-I_uHDA (80 K)
cryst. ice (149 K)
hexagonal ice
$S_{OO}(Q)$
Q (Å^{-1})
(b)
LDA-II (80 K)
cryst. ice (150 K)
cubic ice
$S_{OO}(Q)$
Q (Å^{-1})

(a) TiO_2

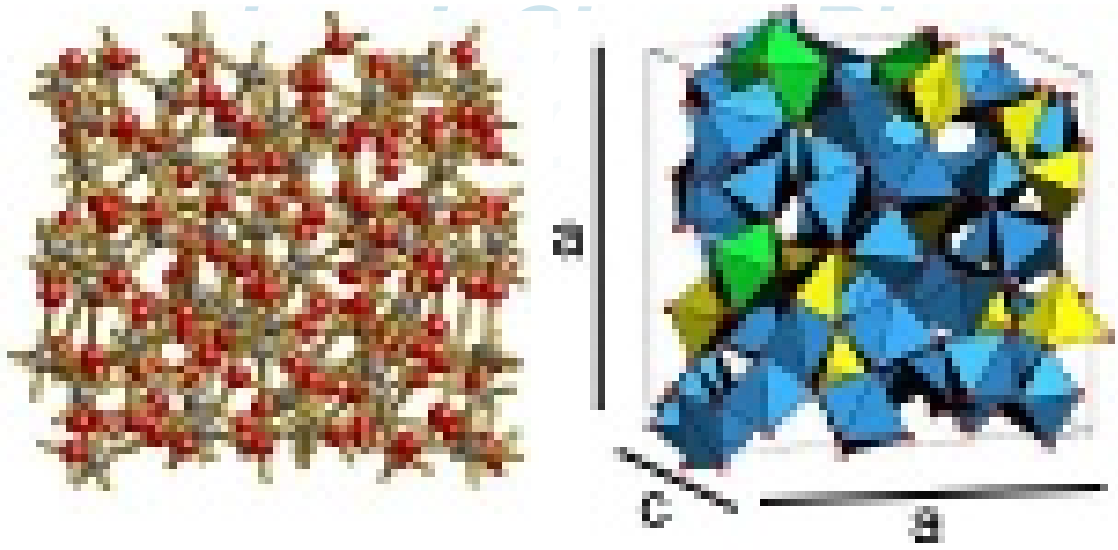

(b) Al_2O_3

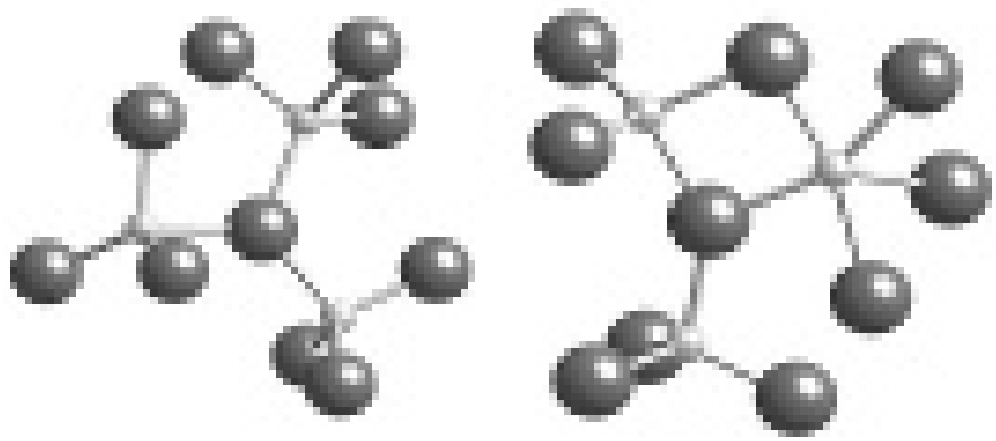

(c)

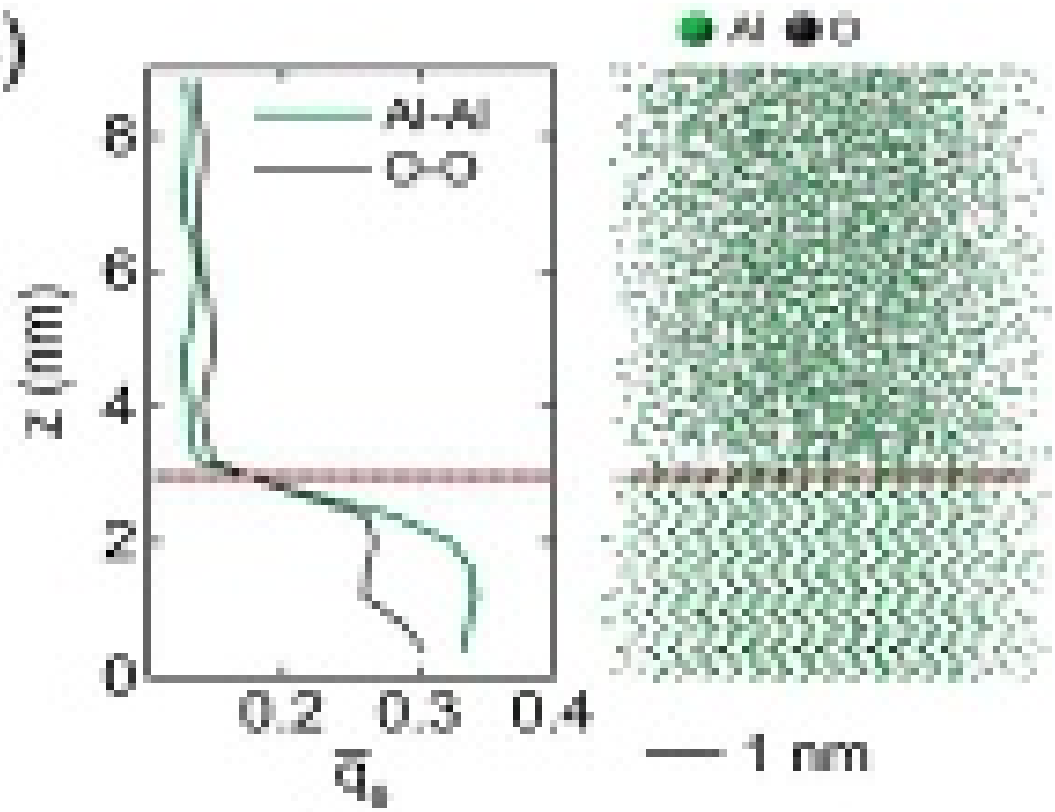

Amorphous Al_2O_3

α-Al_2O_3

(a) VO_2

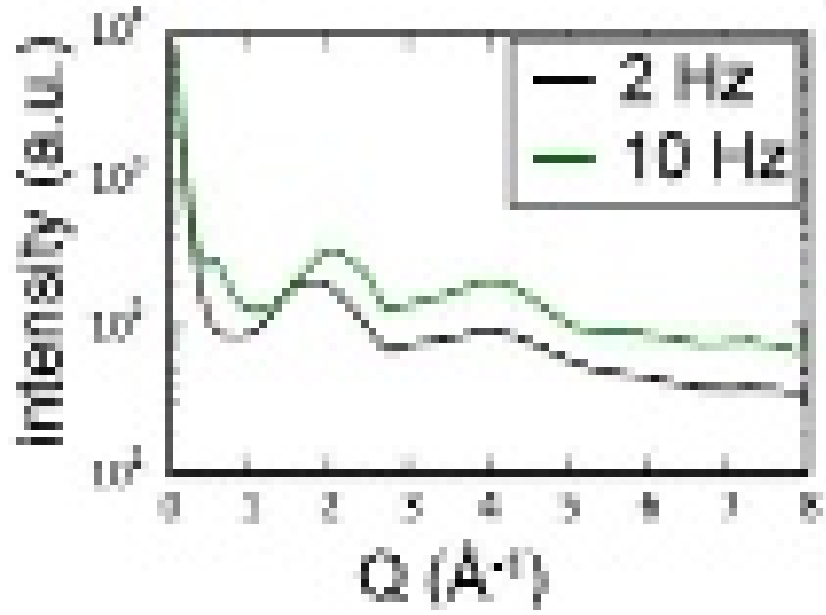

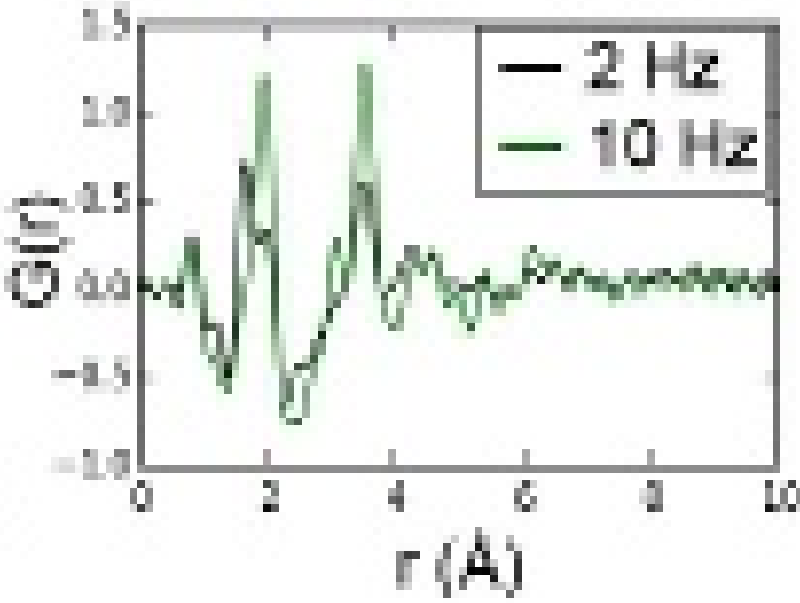

(b) $SrTiO_3$

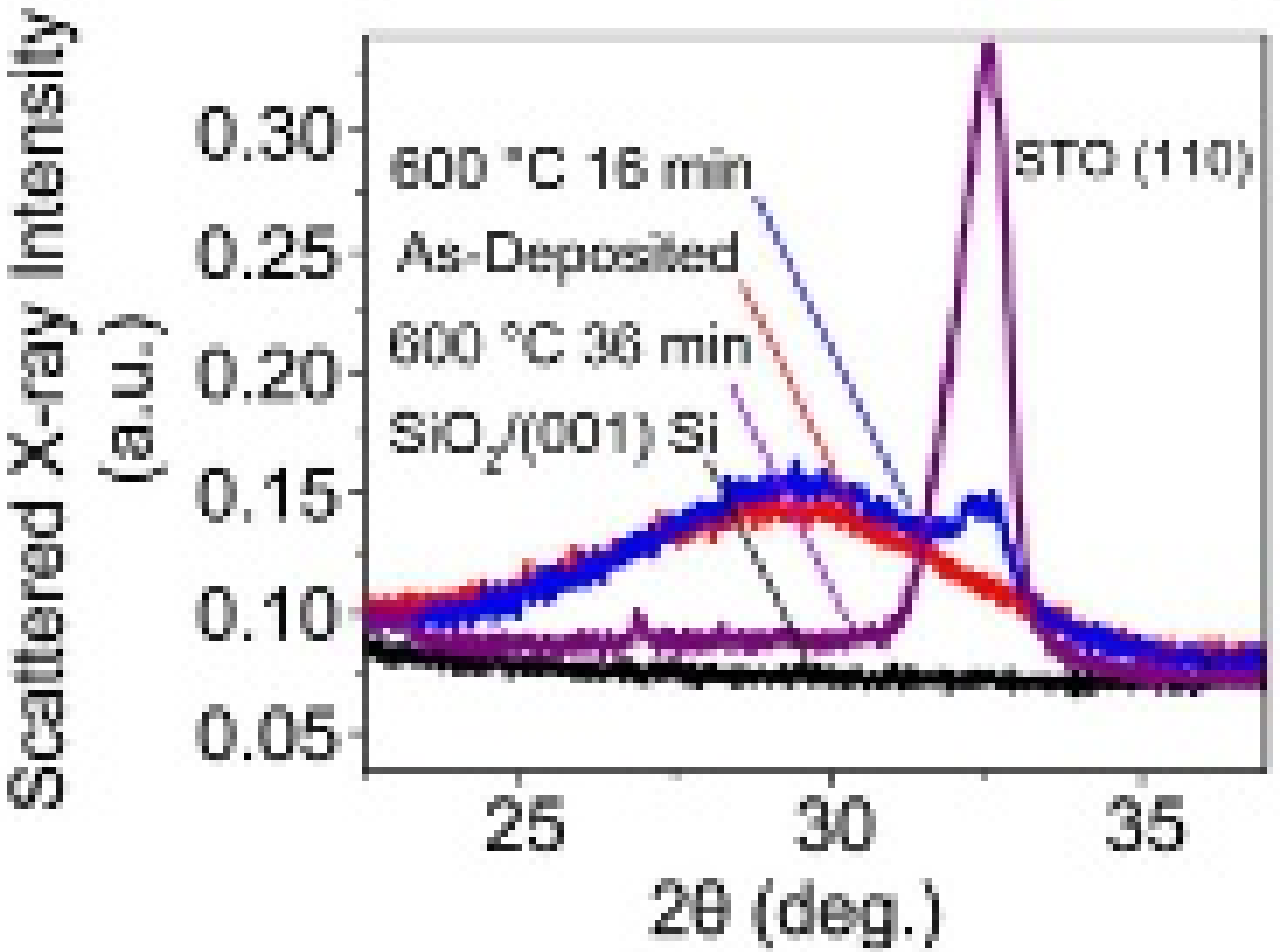

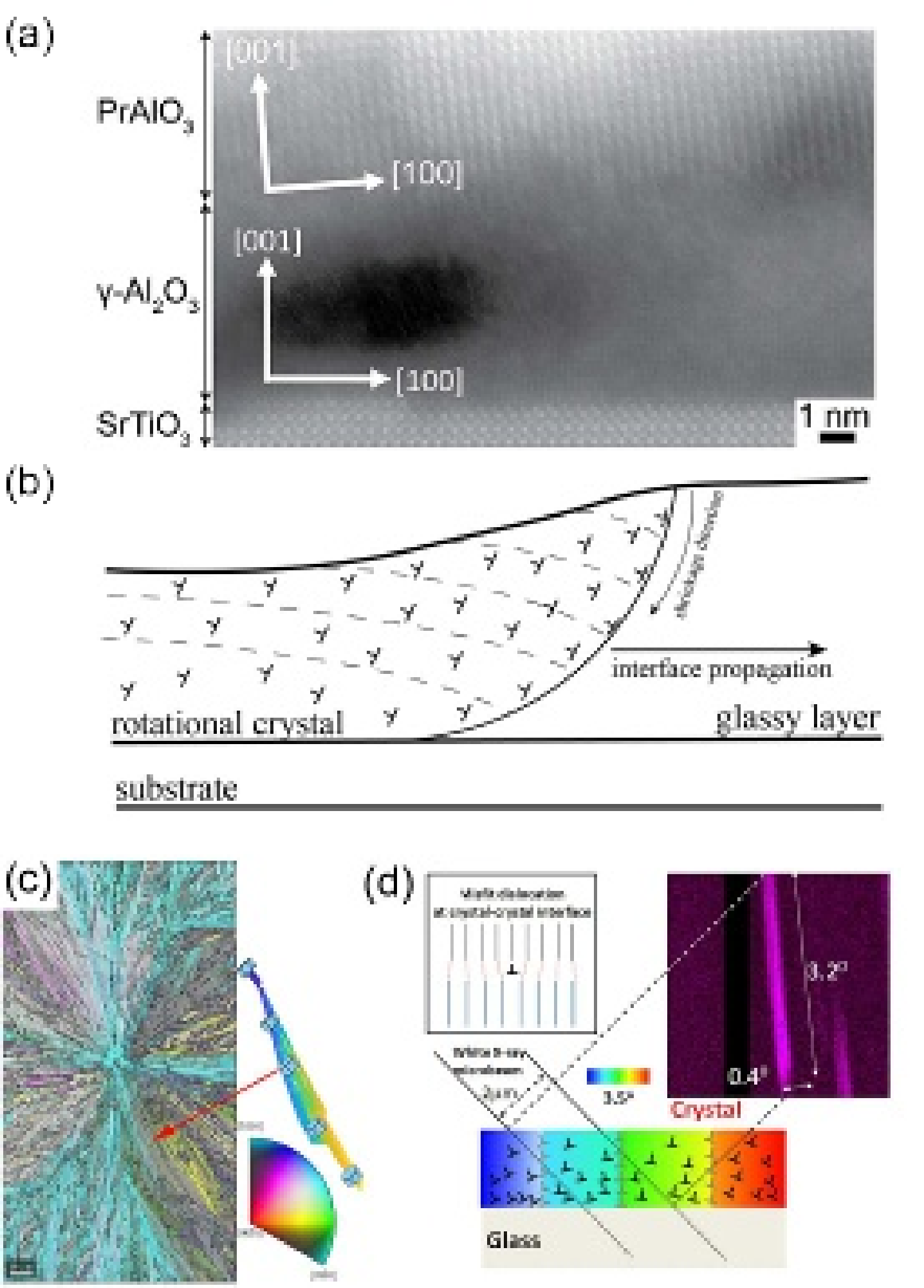
(a)
PrAlO3
[001]
[100]
γ-Al2O3
[001]
[100]
SrTiO3
1 nm
(b)
interface propagation
rotational crystal
glassy layer
substrate
(c)
(d)
3.2°
0.4°
3.5°
Crystal
Glass

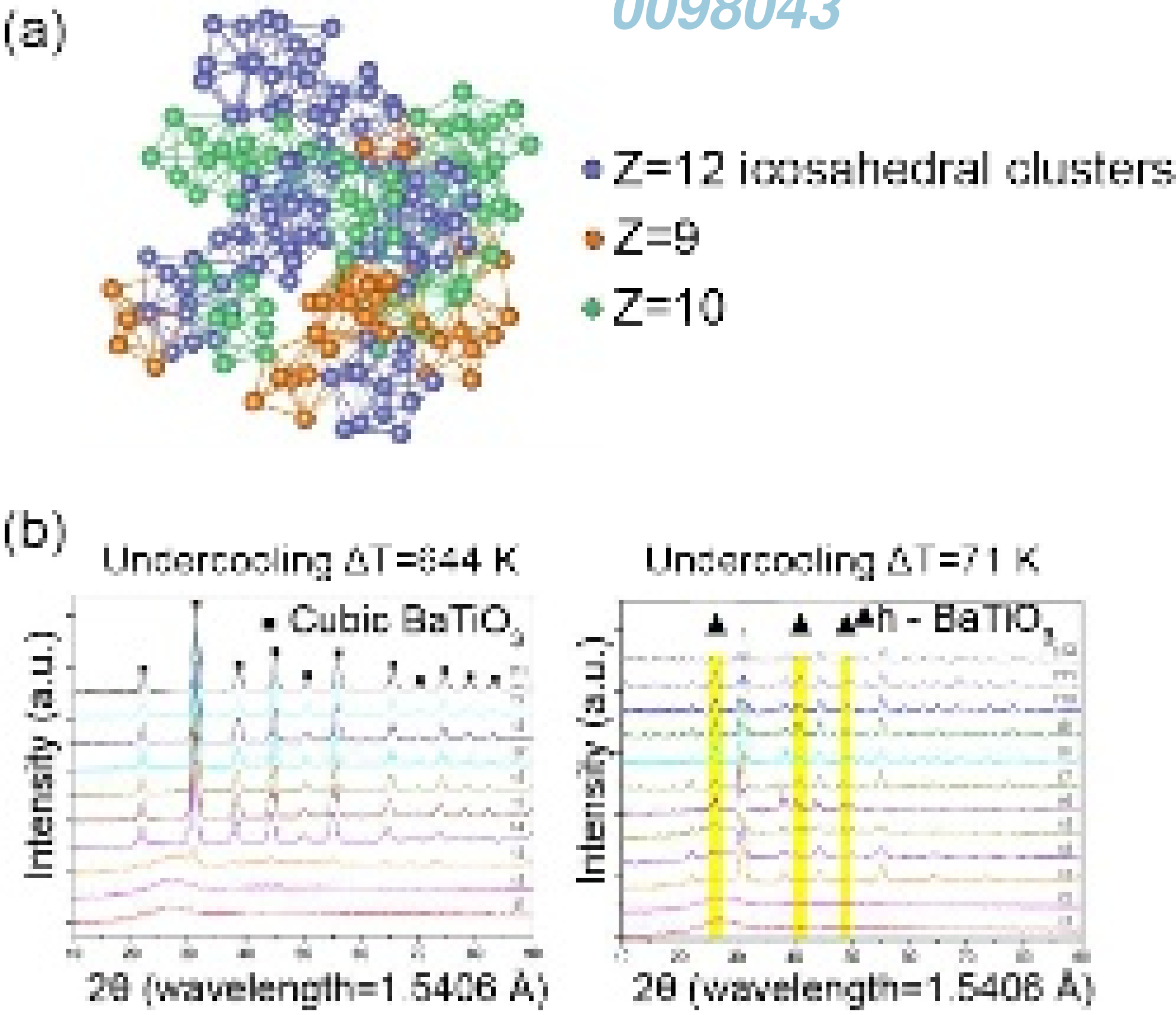

(a)

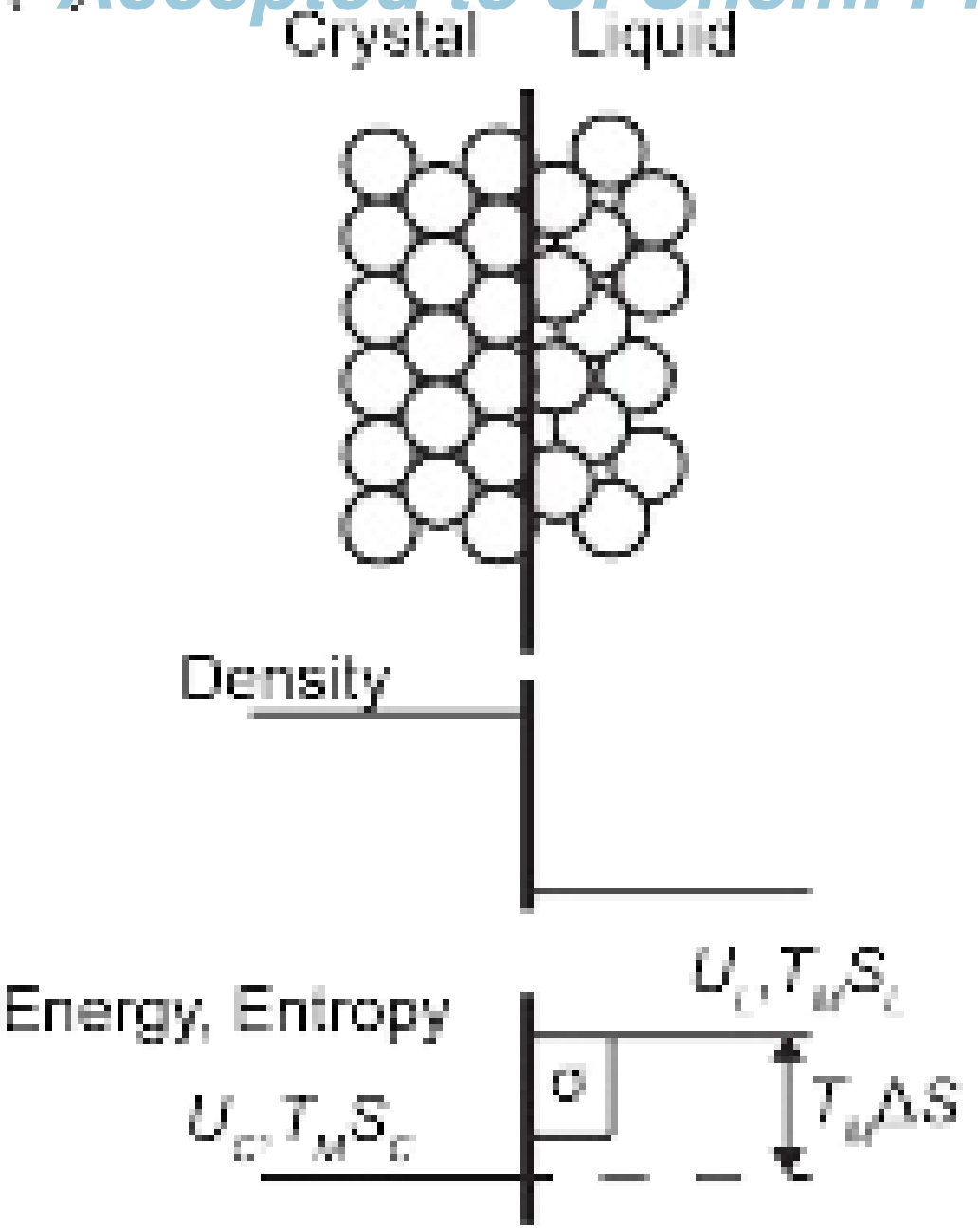

(c)

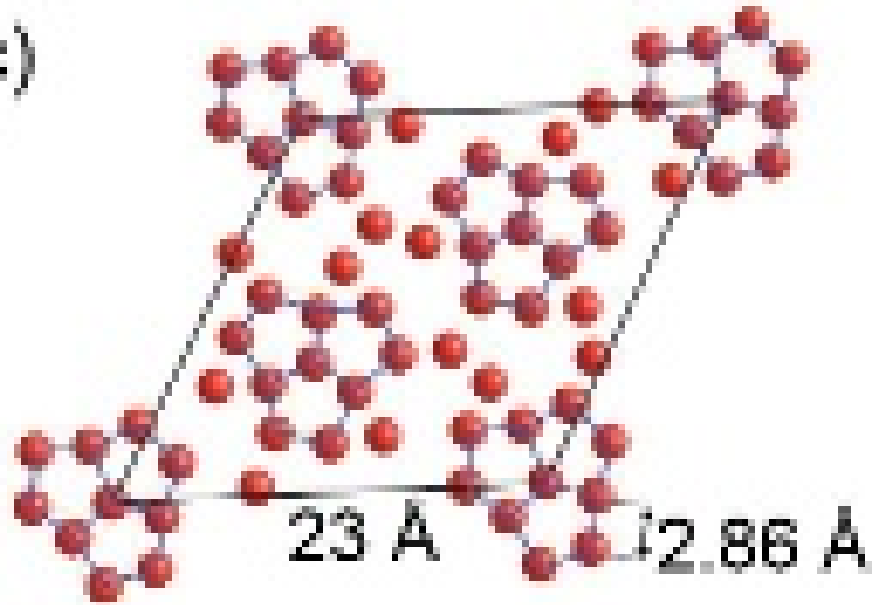

(b)